Hyperspectral remote sensing of soil salinity in Minqin oasis, China

（中国民勤オアシスにおけるハイパースペクトルリモートセシング
を用いた土壌塩分の推定）

Qian Tana

The United Graduate School of Agricultural Sciences
Tottori University, Japan

2018

Hyperspectral remote sensing of soil salinity in Minqin oasis, China

（中国民勤オアシスにおけるハイパースペクトルリモートセシング

を用いた土壌塩分の推定）

A dissertation submitted to

The United Graduate School of Agricultural Sciences, Tottori University
In partial Fulfillment of the Requirements for the Degree of Doctor of Philosophy

Qian Tana

The United Graduate School of Agricultural Sciences
Tottori University, Japan

2018

ACKNOWLEGEMENTS

First of all, I would like to express my deepest gratitude to my principal supervisor Prof. Tsunekawa from Arid Land Research Center (ALRC) of Tottori University for precious academic advising for my research, also enthusiastic help, and strong support for all the time. Great appreciation also given to my co-supervisor Masunaga sensei from Shimane University as well as Prof. Peng who gave me great numbers of valuable suggestions on research design, result analysis, field survey and paper writing. Researching about soil was an impossible mission for a student like me had never learned about soil science before. Because of their encouragement and supports, I can finally fulfil my PhD dream successfully. I also appreciate Professor Kitamura Yoshinobu. He sacrificed a lot of time on helping me figure out my questions about soils and carefully helped me checking my manuscript. I enjoyed the wonderful researches experience with all the professors, which is invaluable wealth for my whole life. Great appreciation also given to Prof. Fujimaki, he taught me about soil knowledge and how to measure the Electivity Conductivity of soil and also borrowed me some equipment.

I would like to thank water resources bureau in Minqin County for sharing important background information and data about water resources in Minqin oasis; the Mr. Wang who is a local farmer and helped me and be the driver during my field survey in Minqin; the local farmers who I have interviewed during field survey in Minqin County for their cooperation.

I would like to thank Professor Xue Xian, Professor Wang Ninglian, Dr. Huang Cuihua, Dr. Liao Jie, Dr. Luo Jun and Dr. Dong Siyang from Northwest Institute of Eco-Environment and Resources, CAS, for providing them with the equipment and the assistance during field survey in China; Professor Wei Huaidong, Professor Ding Feng and Professor Zhou Liping, from Gansu Desertification and Aeolian Sand Disaster Combating Institute for providing them with the equipment and the assistance in the measurement; Professor Kitamura Yoshinobu and Professor Fujimaki Haruyuki from Tottori University for the useful advices and equipment.

Special thanks are given to the members of Plant Production lab and staff of Arid Land Research Center (ALRC) for their help and cooperation in my life. They are Tomemori san, Sakei san, Miyata san, Kobayashi Nobuyuki, Derege, Shunsuke Imai, Du Wuchen, Gou Xiaowei, Chen Xiang, Dagnenet Sultan, Kindye Ebabu, Zerihun Negussie, Fanthun Aklog, Misganaw Teshager, Mesenbet Yibltal, Mulat Liyew, Fekerimaram Asaregew, Shigdaf Mekuriew, Gashaw Tena, Birhanu Kebebe, Getu Abebe. I had a good time with all the lab-members when pleasant exchanging our cultural difference and sharing stories.

I indebted thank to my parents and my grandma who have always supported and always encouraged me. I feel guilty that they are getting old without their beloved daughter and granddaughter's accompaniment. They encouraged and motivated me to finish my study and optimistically face the difficulties in my study and life. I am, so grateful to be surrounded by people I love with all my heart and so thankful for my family and their never ending love and support. I will keep doing my best in my life and bring them more happiness.

I would like to thank to all my friends, who helped and encourage me and spending wonderful fun time with me during my Ph.D.

At last, thanks to myself. It wasn't an easy task for me. I had depression, frustration and self-assurance issues over a long time of my PhD period. However, at the same time I felt challenges, excitement and fulfillment that doing research have brought me with. I think this is unavoidable challenge for a PhD student. I believe that if one haven't been beaten by the toughness and failure over PhD life, she or he perhaps eventually will be physically and mentally stronger for anything might happen in their life. Thanks to myself for not giving up.

Table of Contents

LIST OF FIGURES

LIST OF TABLES

ACRONYMS AND ABBREVIATIONS

ASD	Analytical spectral devices
ASTER GDEM	Aster global digital elevation model
CV	Coefficient of variation
CTI	Compound topographic index
CR	Continuum removal
DEM	Digital elevation model
EC	Electrical conductivity
ECe	EC of saturated soil paste extract, dS/m
$EC_{1:5}$	EC of 1:5 soil and water ratio, dS/m
GIS	Geographical information systems
GRA	Grey relational analysis
HRS	Hyperspectral remote sensing
NDSI	Normalized difference spectral index
NIR	Near infrared
OCC	Organic carbon content
OMC	Organic matter content
PCA	Principal component analysis
PCs	Principal components
SAR	Sodium adsorption ratio
SD	Standard deviation
SI	Salinity index
SWIR	Shortwave infrared
NDSI	Soil salt index
SMC	Soil moisture content
SSC	Soluble salt content
TDS	Total dissolved salt
VIS	Visible infrared
VNIR	Visible-near infrared reflectance
MASL	Meters above mean sea level

Chapter 1

General Introduction

Chapter 1 General Introduction

1.1 Background

Soil salinization is the most common type of land degradation encountered in natural resource management in many parts of the world and has received much attention from farmers, politicians and researchers (Wild, 2003; Rengasamy, 2006; Farifteh et al., 2006; Sheng et al., 2010; Wang et al., 2018). It possesses the potential to cause extensive environmental degradation, health issues and economic welfare. Its occurrence is generally characterized by the appearance of bare salty patches, sparse vegetation cover density, and the appearance of salt tolerant plants and/or the salinization of water resources (Greiner, 1998; Walker et al., 1999). Salinization refers to the process of the accumulation of water-soluble salts in the soil to a level that impacts on agricultural production and environmental health. It commonly occurs as a result of irrigated agricultural practices or long-term changes in water flow in the landscape or changed water management (Pitman and Läuchl, 2002).

Salinization can be caused by natural and/or human activities. In semi-arid and arid land, salinization occurs in one of three situations: salt input increases, freshwater input decreases, or freshwater extraction increases. Under some conditions, all of these processes occur naturally, and in this case are known collectively as primary salinization. For instance, water soluble salts are carried by inland rivers flowing from mountains in upper stream to downstream and form the terminal water bodies. Under drought conditions, salinity of inland waters will increase when decreased precipitation and evaporation results in decreased freshwater input to the soil. In the downstream, without natural outlets, the water bodies fed by river runoff will gradually decreasing in volume and increasing in salinity through evaporation. In this case, it is known as natural or primary salinization process.

Human activity interference leads to the three salinization mechanisms increase rapidly, particularly in dryland and in agricultural systems. Salinization affected by anthropogenic factors is also known as secondary salinization. Human activities that disrupt the hydrologic balance of the soil between water applied (irrigation or rainfall) and water used by crops (transpiration). In many irrigated areas, the groundwater table has raised due to excessive irrigation and the insufficient drainage as well as the removal of indigenous vegetation to make room for cultivated lands and pastures (the decreased demand for groundwater causes the water table to rise). The resource of excessive irrigation are generally comes from the extraction of freshwater from inland bodies (surface runoff and/or groundwater) which reducing the lake area and further concentrating salts (Nurmemet et al. 2015). The accumulation of soluble salts in the root zone greatly affects plant growth, resulting in lower crop production and adversely affecting the soil fertility. As one of the primary inhibitors of agricultural production and ecosystem, salinization might ultimately lead to environmental disaster and food crises in arid lands (Munns, 2002; Barrett-Lennard, 2003).

Soil salinity is defined as the salt content in the soil. Salinity in water can be measured in two ways: total dissolved solids (TDS) and electricity conductivity (EC) of a saline solution. The metric unit for conductivity is the deci-Siemens per meter (dS/m) (Paul and Rashid, 2016). The excess salts in the soil solution are comprised largely of the chloride and sulfate anions and sodium, magnesium, and calcium cations (Qingfeng Lv et al., 2018). It results in poor plant growth and low soil microbial activity due to osmotic stress and toxic ions (Yan et al., 2015). Threshold value of soil salinity classes deleterious effects occur can vary from one environment to another depending on several factors including plant type, soil-water regime and climatic condition (Maas et al. 1986). According to FAO 1985, the soil is said to be non-saline if the saturation extract water contains less than 3 grams of salt per litre or 4.5 mmhos/cm, and the soil is said to be highly saline if the salt concentration of the saturation extract contains more than 12 g/L. However, based on Albert (Canada) Agriculture and Forestry, non-saline soils are defined as EC of salt solution <2 dS/m, and strongly saline soils are the soils have EC >8 dS/m, very strongly saline soils have EC >16 dS/m. Therefore, site-specific classification is needed (Paul and Rashid, 2016).

Salinization has become a serious threat to the agriculture and the livelihood of residents in the arid north western China. Their agriculture is heavily rely on the river system. Growing soil salinization and severe water scarcity and are closely related problems that are strongly affecting agricultural development and sustainability. The low precipitation is coupled with intensive evaporation and ineffective irrigation drainage systems have resulted in secondary salinization (Ma et al., 2005; Wang et al., 2008).These problems are especially severe in oasis ecosystems, where the water scarcity and soil salinization have caused an unrepairable loss of productive land within the past few decades and have threatened the sustainability of agriculture and ecosystem stability.). Among the numerous inland river basins in the Northwest China, the lower reach of the Shiyang River Basin is well-known for its serious water shortage and the deteriorated eco-environment, which have impeded the social and economic development (Wang, 2009). Minqin oasis, in the lower reaches of the Shiyang River (an inland river rising in the Qilian Mountains), suffers a great shortage of fresh water for agriculture because of the low rainfall and massive demand for water created by increased agricultural activity and rapid population growth. Groundwater has been over-exploited to fill the gap between surface freshwater supply and demand (Bondes and Li, 2013; Wei, 2016). Groundwater extraction provides short-term relief from the scarcity of water for agricultural and domestic use, but excessive extraction lowers the water table and increases salt concentrations in groundwater (Chen et al., 2016). Long-term agricultural use of saline water has led to a rapid increase of secondary salinization at Minqin oasis (Chen et al., 2016; Qian et al., 2017). For example, the total area of saline land within Minqin oasis increased by 541.35 km^2 from 1991 to 2009 (Xiao et al., 2007; Zhang et al., 2014). Moreover, the persistent water scarcity and adverse effects of secondary salinization on crop yields led to the abandonment in 2003 of about 780 ha of cropland (equal to 81% of area under cultivation) at two villages at Minqin oasis (Ma et al., 2007).

1.2 Literary review

1.2.1 Salinization in the world

Soil salinization is a universal problem, especially in much of the waterfront, arid and semi-arid lands of more than 100 countries and regions over different continents (Table 1). Irrigation-induced land salinization has put serious risks to the sustainability of irrigated agriculture (Singh et al., 2012). Arable land affected by salts accounts for 23% of global arable land (Scudiero et al., 2016). About 17% of the global cropland is under irrigation, but irrigated agriculture accounts for over 30% of the total production (Hillel, 2000). Therefore, secondary salinization is of major concern for world food production. An estimations of the proportion of secondary salinization soils to its irrigated for several countries are 8.7 % for Australia, 15% or China, 16.6 % for India, 23 % for USA, 33 % for Egypt, 33.7 % for Argentina, and 60% for Uzbekistan in 1980's and 1990's (Paul and Rashid, 2016). What's worse, salinization and related problems has enlarged considerably during the last few decades with a spreading rate of 2 million ha per year due to the speedy expansion of irrigation (Singh, 2010; Singh, 2011).

In Australia, 16% of the cropping area (7.6×10^6 km) is likely to be affected by water table-induced salinity, 67% of the area has a potential for 'transient salinity, costing Aus$1330 million per annum. In recent years, many farmers have abandoned their rice fields due to the adverse impact of soil salinization (Rengasamy, 2006).

In Pakistan, an estimates show that 25% and 40% of the irrigated lands in the Punjab and Sindh are salt-affected respectively, which impacts on the livelihoods of about 10–20 million people and ecosystem (Barrett-Lennard and Hollington, 2006).

Soil salinization restricts agricultural development, especially when sustainable agricultural development and environmental quality improvement strategies are being considered. In Bangladesh, due to increasing degree of salinity and expansion of affected areas normal agricultural land use practices become more restricted (Karim et al., 1990). Large area of the coastal and off-shore lands of arable lands are affected by varying degrees of salinity (Asib, 2011). Though salinity mapping, a research showed that, saline and highly saline areas covered about 3336.67 hectares and 2941.94 hectares respectively which are 41.46% and 36.69% land of total study area of their study sites (Mohamed et al., 2012).

Table 1 World distribution of salt-affected soils

Continent	Total Area (millions ha)
North & Central Asia	211.7
Southeast Asia	20
South Asia	85.1
North America	15.8
Central America	2
South America	129
Africa	80.5
Australasia	357.4
Europe	30.7
Total	932.2

Reproduced from Sumner Szabolcs, 1989.

1.2.2 Method and techniques of retrieving soil salinity

Even though the effects of spatiotemporal variations of natural conditions (e.g., availability of irrigation water) and the temporal changes of agricultural practices have made it difficult to monitor and manage the salinization, the accurate estimations of the areal extent of salt affected soil and prediction of areas has potential to become saline are essential for policy makers, planners and farmers to allow effective management of irrigated land, control of salinization and reversal of current trends of soil and water degradation. Thus, it is crucially important to monitor soil salinity and assess its severity to prevent further degradation of agricultural land (Weng et al., 2010).

Conventionally, soil salinity has been measured by collecting in situ soil samples and analysing those samples in the laboratory to determine their solute concentrations or electrical conductivity (EC). EC can be measured in saturated paste extracts (ECe) or by using extracts with different soil-to-water ratios (Shainberg and Levy, 2005). Because the conventional methods of monitoring salinity by using ground-based geophysical techniques are time-consuming and costly (Dehaan and Taylor, 2003) soils have high spatial variability, many researchers have attempted to develop more cost-effective approaches by utilizing remote sensing techniques to monitor the salt-affected soils and predict the potential salinization (Metternicht and Zinck 2003; Farifteh et al. 2007; Mulder et al. 2011).

Remote sensing uses the electromagnetic energy reflected from targets to obtain spectral information about the land surface in details. Spectral information enables the identification of object based on its spectral features such as reflection, absorption, and/or emit of electromagnetic energy at specific wavelengths. Compared with limit band numbers and resolutions of multispectral remote sensing techniques, hyperspectral remote sensing techniques have hundreds of bands, long wavelength, and high spectral resolution. It can capture subtle differences in soil properties and provide quick indirect assessments of soil characteristics such as salinity, organic content and moisture content (Ben-Dor and Banin, 1995; Farifteh et al., 2006; Gomez et al., 2008; Haubrock et al., 2008; Zornoza et al., 2008; Ben-Dor et al., 2009; Goetz, 2009). Because the reflectance spectra of soils can provide quantitative information about the particular salt minerals in soils, the development of methods that use hyperspectral data to estimate soil salinity has been the objective of many studies during the past two decades (Farifteh et al., 2006; Gomez et al., 2008; Haubrock et al., 2008; Lu et al., 2013). Hyperspectral visible and near-infrared reflectance spectroscopy displays promise as a result of its performance, accuracy and cost effectiveness in the determination of most soil properties in laboratories (Shepherd and Walsh, 2002).

Soil spectral reflectance is affected by many soil properties such as parent material, types of soil texture, soil moisture, salt content, colour, surface roughness, organic matter content, particle size, iron oxide content and texture (Farifteh, 2007), vegetation cover, vegetation types and vegetation growth conditions (Weng and Gong, 2006).

The dynamic processes of salinization also affect the spectral, spatial and temporal behaviour of the soil salts. The spectral reflectance of features vary with the change of those affecting factors, including salt crusts and efflorescence besides variations in surface texture and structure. Schmid et al. confirmed the fact that saline soil reflectance results from spectral properties such as the presence of salt crust, soil colour and moisture content, which have a combined effect on the amount of reflectance and also found that crusted saline soil reflects strongly in the visible and near-infrared (NIR) bands. Spectral reflectance of soil salt features can be promising surface indicators of soil salinity and spectral-based models can be generated to predict or mapping salinization. Fernandez et al. used the correlation between surface colours, EC and the sodium adsorption ratio (SAR) to predict soil salinity. This is based on the fact that the capabilities of different salt minerals to reflect and absorb light at particular band regions of the electromagnetic spectrum (Mougenot et al., 1993; Metternicht and Zinck, 2003).

Single or multiple wavebands that are sensitive to soil salinity in those areas of the spectrum can be mathematically combined (e.g., in ratio form, normalized ratio form, normalized difference form) into indices that can be used for modelling, detecting and mapping of soil salinity as well as other unidentified parameters (Douaoui et al., 2006). A number of researchers have developed different salinity indices to detect and map soil salinity such as Normalized Difference Salinity Index and Salinity Index (Allbed and Kumar, 2013). Empirical models based on those indices can be used to predict salt concentrations in soil (Farifteh et al., 2007).

However, the complexity of soil properties makes identification of salt minerals in soil difficult and limit the monitoring and assessment of the salinization (Csillag et al.,1993), compounded by the fact that halite has an essentially featureless spectrum in the optical wavelength (Crowley, 1991). The spectral features that can vary according to the dominant salt present (e.g., NaCl or $CaSO_4$), the sampling season and the area sampled (Metternicht and Zinck, 1997; Farifteh et al., 2007), which makes it difficult to define a general model that is applicable across large areas (Chang et al., 2001; Ben-Dor et al., 2002; Weng et al., 2010; Fan et al., 2015). The above shortcomings indicate that detecting and mapping soil salinity in arid and semi-arid regions using remote sensing is remain challenging.

1.4 Aims of the research

This research aims at quantifying soil salinity in soils on the basis of the use of soil reflectance and field survey, and investigate the potential of field and lab-derived spectra for estimation salinity through comparison.

The specific objectives of this research are:

(a) To establish spatial distribution of soil salinity and analyzing its casual factors and to evaluate the effect of land use practices on the regional scale salinization;

(b) To quantitatively estimate soil salinity by modeling from lab-measured spectral reflectance data;

(c) To quantitatively estimate soil salinity by modeling from field-measured spectral reflectance data.

1.5 Structure of thesis

The thesis is organized into 5 chapters. After this introductory chapter, Chapter 2 (Study 1) detects the spatial variation of soil salinity and its causal factors in Minqin oasis. Chapter 3 (Study 2) derives the salt content in salinized soil from lab-hyperspectral reflectance data. Chapter 4 (Study 3) derives the salt content in salinized soil from field-hyperspectral reflectance data. The last chapter, Chapter 5, provides summarize of previous chapters. It includes conclusions, limitations of the study, and future research.

Fig. 1 The integrated methodology of the thesis

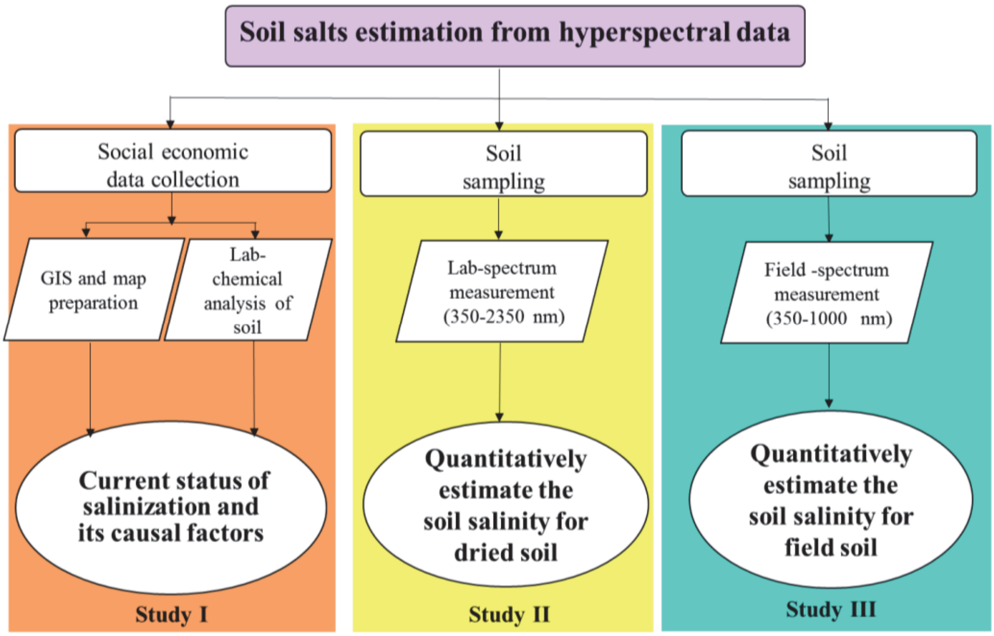

1.6 Study area description

1.6.1 Location

Minqin oasis is administratively named Minqin County of Gansu Province, northwestern China. The total area of Minqin County is about $1.6*10^4$ km^2 and lies between 103°02'E and 104°02'E, and between 38°05'N and 39°06'N. The Huqu region is located on the downstream alluvial plain of the Shiyang River basin, in the northern part of the Minqin oasis. The terrain is relatively flat, with an elevation that ranges from 1254 to 1376 masl. It covers an area of 1430 km^2 and is located between 38°42'N and 39°10'N, and between 103°19'E and 103°49'E (Fig. 2-a). The region is surrounded by the Badan Jaran Desert to the west and north, and by the Tengger Desert to the east.

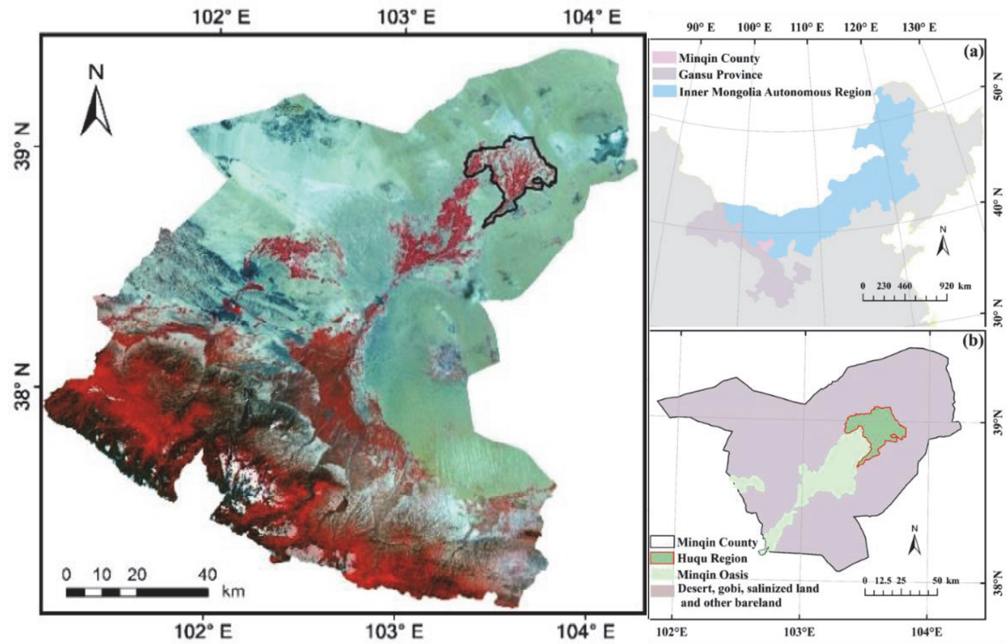

Fig. 2 (a) The location of the study area (the Huqu region) within China, (b) Locations of the 94 soil samples analyzed in the present study.

1.6.2 Climate

The region belongs to desert-oasis ecotone and has a temperate continental arid climate with more winds in winter and spring. The mean annual temperature is 7.8 °C with monthly means range from -8.6°C in January to 21.8°C in August. The frost-free period is 189 days roughly during April to October. The growing season for vegetation including crops are from March to October. The total annual precipitation averages 110 mm occurring in the summer months, but the potential evaporation ranges between 2000 and 2600 mm. The mean annual wind speed is 2.8 m/s, but the highest wind speed can reach 23 m/s, and winds strong enough to entrain sand occur 139 days per year on average (Local chronicles office of Minqin Count, 2014).

Table 2 Monthly mean temperature and mean precipitation of Minqin County

Month	1	2	3	4	5	6	7	8	9	10	11	12
Temperature (°C)	-8.6	-4.6	2.2	10.6	16.7	21	23.2	21.8	6.1	8.3	-0.1	-6.5
Precipitation (mm)	0.5	1	2.8	4.7	10	15.9	23.8	28.1	17.2	6.9	1.6	0.5

1.6.3 Soil and vegetation

The main soil types are grey-brown desert soil, sandy soil, solonchak (similar to the salinized soils in the Aridisol order of the U.S. Soil Taxonomy), meadow soil, and anthropogenic-alluvial soil (Danfeng et al., 2006). The main soil type in croplands is a silty clay or a sandy silt. Grey-brown desert soil mainly distributed at the areas out of the oasis such as mountain that lower than 1500 m, denudation monadnock, pluvial fan. Sandy soil has a wide distribution all over the oasis and formed from Aeolian accumulated parent material. Solonchak are formed from saline parent material under conditions of high evaporation conditions encountered in closed basin under warm to hot climates with a well-defined dry season in arid zone. Solonchak has a high soluble salt accumulation within 30 cm of the soil surface. Solonchak widely spread over the Minqin oasis and cover an area of 1168.66 km^2.

Native vegetation includes drought-resistant shrubs, salt-resistant shrubs, and perennial sand-loving herbaceous plants (e.g., Elaeagnus angustifolia, Populus euphratica, Salix purpurea and Agriophyllum squarrosum) (Kang et al., 2004). Because most of the grassland area in the oasis was suitable for cultivation, very little natural grassland remains; however, sparse grassland has developed where cultivated land was abandoned for more than decades.

1.6.4 Hydrology

Groundwater development was very limited until the middle 20th century. The groundwater was mainly recharged by surface water via river infiltration, canal system seepage, and farm irrigation return flow, while the discharge was via evapotranspiration (becoming less and less because of declining groundwater table) and artificial abstraction.

Since the 1950s, intensive development and irrigated agriculture using both surface and groundwater was facilitated by the building of the Hongyashan Reservoir. In 1965 there were only 165 shallow wells but by 1976 there were 10,000 wells at maximum by the end of the 90’s to a maximum depth of 320 m. The main irrigation water resources in the oasis are surface water from the reservoir and groundwater and the only remaining surface water body is the Hongya Mountain reservoir. A network of irrigation canals with a length reached up to 3,084.5 km was built to delivering water to irrigated croplands. As a result, groundwater had been intensively extracted to meet demands for irrigation and industry, which led to the groundwater levels decline continuously. The groundwater table was at a depth of 2.7 m below the ground surface and decrease to about 19 m below the ground surface at 2012 (Fig. 3-b). The groundwater level of Huqu region declined from a depth of 10.328 m in 1998 to 16.409 m in 2014 (Fig. 3-c). Due to surface water shortage, groundwater recharge from surface water greatly declined, which led to the groundwater quality degradation (mineralization). The total dissolved salts in underground water of Minqin County increased from 1.9843 g/L in 1998 to 2.5762 g/L in 2012 (Fig. 3-d).

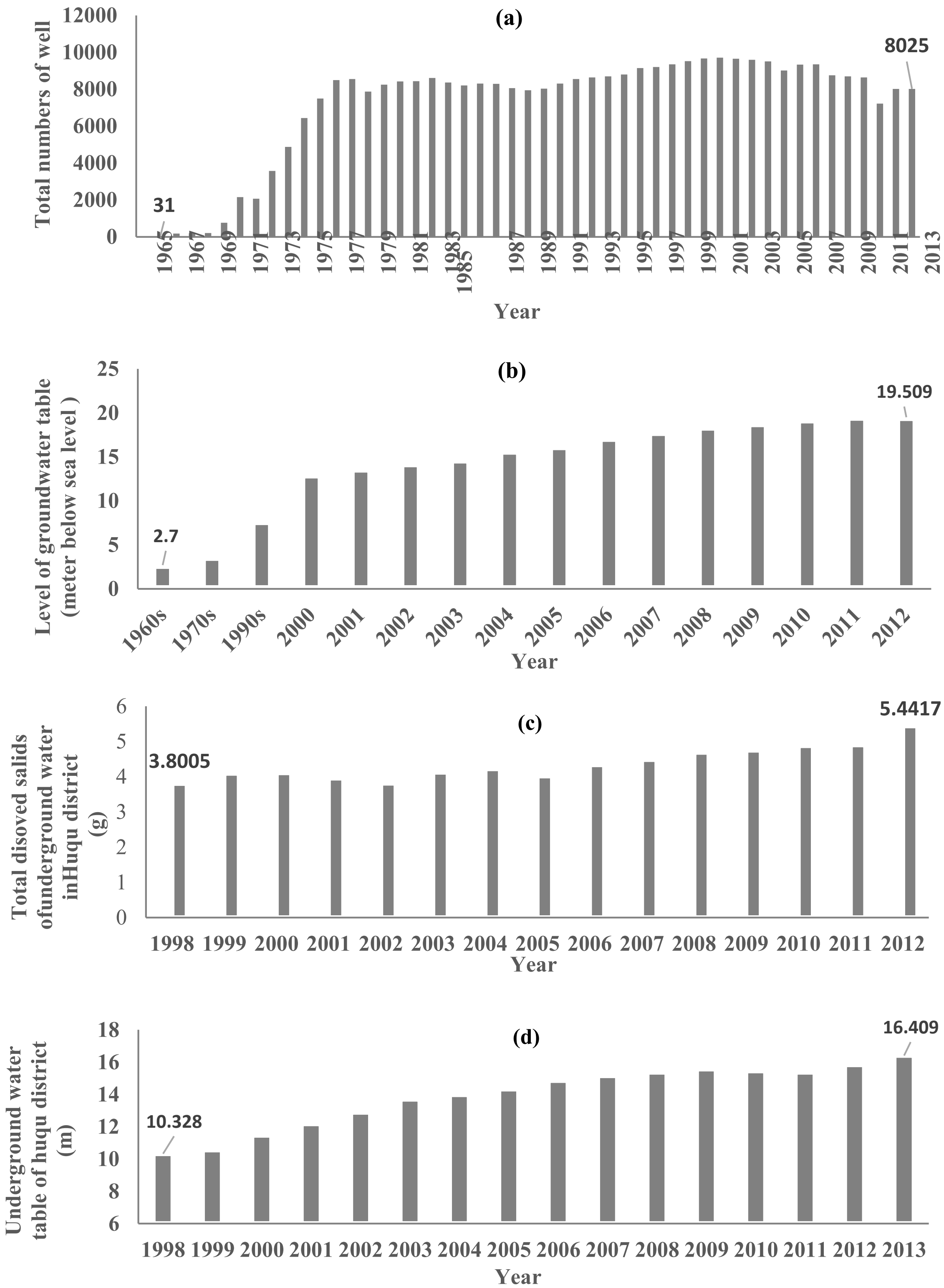

Fig. 3 (a) the total number of well in Minqin County; (b) the ground water table level of Minqin County (c) the ground water table level of Huqu region; (d) the total dissolved salt of ground water of Minqin County.

1.6.5 Social economy conditions

The Minqin County is administratively divided into 18 sub-towns includes Dong Hu, Xi Qu, Shou Cheng, Hong Shaliang, Quan Shan, Da Tan, Shuang Cike, Dong Ba, Yang Lu, Su Wu, San Lei, Da Ba, Xue Bai, Chang Ning, Chong Xing, Cai Qi, Nan Hu and Hong Shagang.

The Minqin oasis is divided into five sub-regions based on the historical and geological distribution and utilization of river: the Huqu, Baqu, Shoucheng, Hongsha Liang and Quanshanqu regions. Huqu region consists of two sub-towns which are Dong Hu, Xi Qu and Shou Cheng.

Though the ecological condition of Minqin County was fragile, the population increased to 307,200 in 2004, increasing by 107,468 compared to 1949. At the same time, farm population increased from 193,209 to 248,600Total population in Minqin County is 0.3 million with a population density of 272.8 persons/km^2 in 2009. More than 0.2 million population (74.5%) are living in villages. Minqin oasis has an agriculture history of more than 2000 years. The main livelihood are irrigation farming and livestock. The major crops include cereals (spring wheat, summer maize) and cash crops (cotton, melon, and fennel).

1.6.6 Environmental issues

The location of the Huqu region and the use of inappropriate irrigation practices there has led to protracted and severe groundwater mineralization, soil salinization and desertification, such that much of the cropland can no longer sustain grain crops. Substantial cropping areas have been abandoned because of low productivity due to groundwater mineralization (groundwater mineralization > 3.0 g/L can cause yield reductions of >10%) (Xiao et al., 2007). We chose the Huqu region as our study area because of the existence of both the original salt accumulation (primary salinization) and irrigation-caused salt accumulation (secondary salinization). The area has been suffering from severe ecological problems for decades, including high mineralization of groundwater, salinization, and desertification characterized by sand invasion, as well as from social and economic pressures caused by ecological emigration and cropland abandonment.

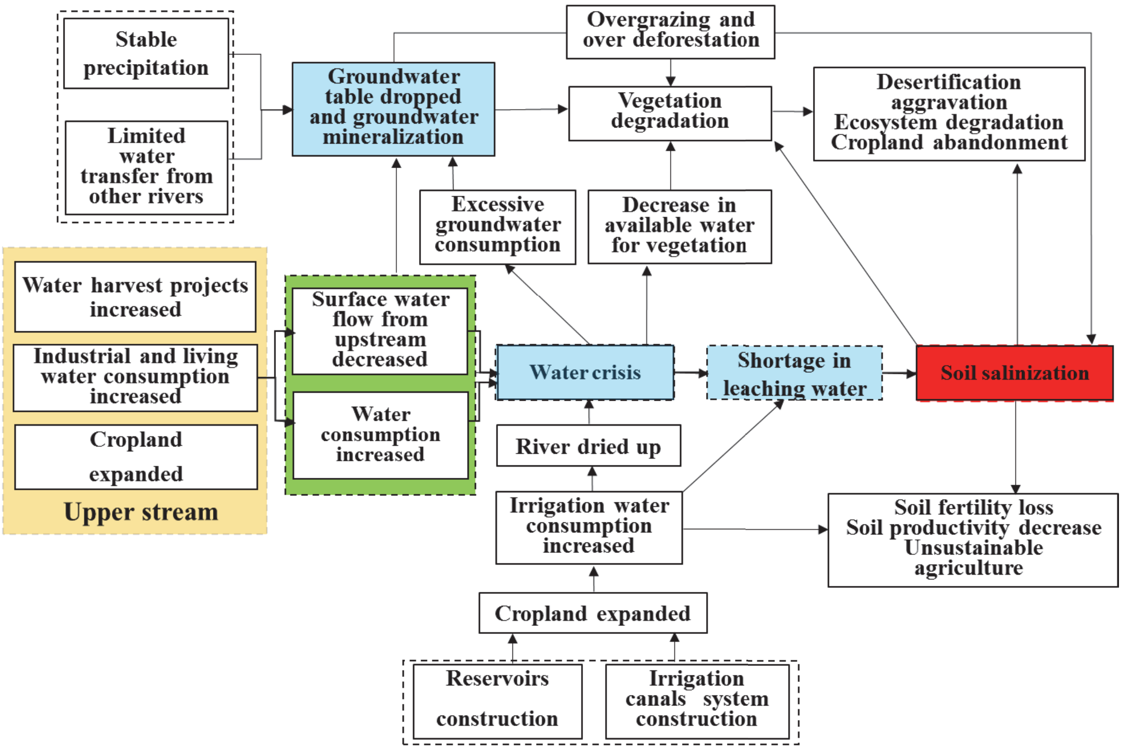

Fig. 4 The summary of salinization process in Minqin oasis.

Chapter 2

Spatial variation of soil salinity and its causal factors in Minqin oasis

Chapter 2 Spatial variation of soil salinity and its causal factors in Minqin oasis

2.1 Objectives

Because of its severity, land salinization has received much attention from researchers. Although the salinization is affected by many factors (Rengasamy, 2006), the interaction among the factors responsible for different types and intensities of salinization of different land use and cover types is still inadequately understood. To provide this information, we began a study of the Minqin oasis. Our main objectives were to (a) analyze the spatial variability of soil salinity, (b) analyze the factors that affect soil salinity, and (c) rank the importance of these factors based on land use and cover types. To accomplish these goals, we applied the technique of grey relational analysis to the field survey data, supported by geographical information system (GIS) tools. We also took advantage of government statistical records and remote sensing data in our statistical analysis and relational factor analysis.

2.2 Materials and methods

2.2.1 Study site

The Huqu region is located on the downstream alluvial plain of the Shiyang River basin, in the northern part of the Minqin oasis. The terrain is relatively flat, with an elevation that ranges from 1254 to 1376 masl. It covers an area of 1430 km^2 and is located between 38°42’N and 39°10’N, and between 103°19'E and 103°49'E.

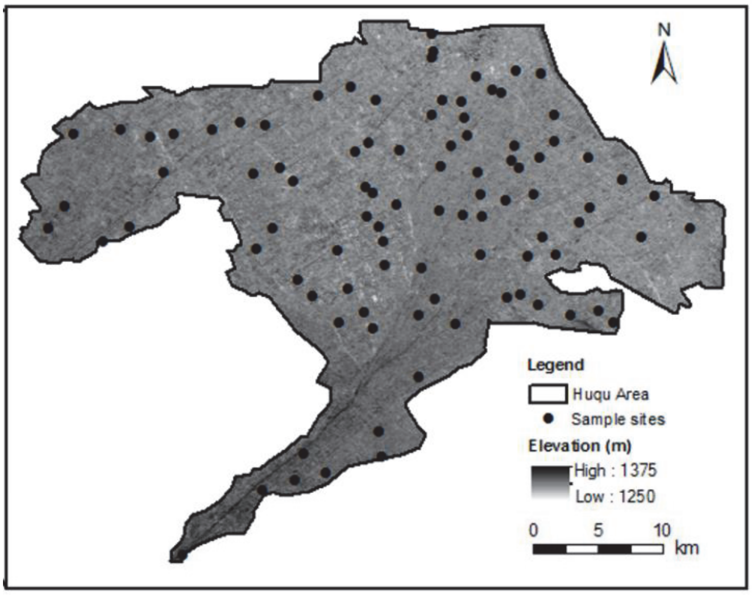

Fig. 5 Locations of the 94 soil samples analyzed in the present study

2.2.2 Soil sampling

The field dataset was obtained during April 2015, when the salt concentration in surface soils reaches its maximum in this region. In April, the low precipitation combines with a high evaporation rate to cause salt from deeper soil layers to migrate upwards and accumulate near the surface of the soil (Elnaggar and Noller, 2009). We obtained 94 surface soil samples (Fig. 2-b) to a depth of 10 cm from unused land (9 samples from shrubland, 5 samples from abandoned land, 46 samples from sparse grassland, 13 samples from saline wasteland) and cropland (used to grow wheat, sunflower, alfalfa, goji berry, and fennel). The sites were selected based on the results of previous soil salinity studies and Google Earth images, and each sample site represented an area of 90 m ×90 m. For each sample point, we combined five topsoil samples into a single composite sample, which we used to represent the value of the soil chemical parameters at that site. The location of each sample point was recorded with a MAP64SJZ GPS receiver (Garmin, Olathe, KS, USA) and we photographed the site. The characteristics of the soil surface, the land use and cover types surrounding the site, and the vegetation cover were recorded in a field notebook. We also consulted local farmers to learn about historical land use and cover types.

2.2.3 Laboratory analysis

Soil moisture was assessed during the soil sample collection. The samples were sealed into weighed, empty specimen boxes and their total weights were measured. When we returned to the laboratory, we opened the boxes and oven-dried the samples for 24 hours at 105 °C together with the boxes. We calculated the soil moisture content (SMC) as a percentage of the dry soil weight.

For the chemical analysis, the samples were air-dried, crushed, and passed through a 1-mm sieve to remove large particles and plant residues. To quantify the soil salinity, we measured the electrical conductivity ($EC_{1:5}$) in deionized distilled water at 1:5 g/ml soil:water ratio. The standard methodology for the soil salinity assessment needs to measure the EC from the soil saturated paste extract, which is cumbersome and tedious. One of the most widely used soil over water mass ratios is 1:5. An Investigation of the relationship between the ECe with the $EC_{1:5}$ for soils in Greece showed that the mean ECe is about 6.5 times larger than $EC_{1:5}$ with a linear model of $ECe = 6.5318\ EC_{1:5} - 0.1088$ ($R^2 = 0.9317$) (George K. et al., 2018). However, the coefficients of their relationship vary according to the area of interest.

We calculated the frequency distribution of these values and several associated parameters: the mean, median, standard deviation, skewness, kurtosis, range, and maximum and minimum values. We used version 23 of the SPSS software (www.ibm.com/analytics/us/en/technology/spss/) for our statistical analysis.

We also measured the soil pH. To make the pH measurements better reflect the water content of the soil under field conditions, we used a 1:1 g/ml soil solution (Thomas G.W. et al., 1996).

2.2.4 GIS and map preparation

Maps of the distribution of soil $EC_{1:5}$ were prepared to visualize the results at the 94 sample sites. We used version 10.2.1 of the ArcView software (www.esri.com). We also visualized the layout of the irrigation canal network, depths to the water table, and

TDS data for the water using ArcView. Additional data included an ASTER Global Digital Elevation Model (ASTER GDEM) acquired from https://gdex.cr.usgs.gov/gdex/ at a 30-m resolution. To describe the topographic characteristics of the sample sites, we derived the compound topographic index (CTI), which is widely used in hydrology and terrain-related applications, from the ASTER GDEM data (Beven and Kirkby, 1979). CTI is a compound index that is calculated using two primary topographic attributes (Moore I.D., Grayson R.B. and Ladson A.R, 1991); it is also known as the steady-state wetness index when it is used to quantify the catenary landscape position (Gessler et al., 2000). The following equation was used to calculate the CTI values

$$CTI = \ln (\alpha / \tan\beta) \tag{1}$$

Where α represents the catchment area per pixel, and β represents the slope gradient. Low CTI values represent small catchments, steep slopes, and upper catenary positions. High CTI values represent large catchments, gentle slopes, and lower catenary positions with a higher capacity for water accumulation and wetness (Marthews, T.R., 2015).

2.2.5 Grey relational analysis

A grey relationship is a relationship among different types of data series often with different units of measurement when there is considerable uncertainty and an unsatisfactory sample size (Huang J., 2011). Grey relational analysis (GRA) is a way to identify the key factors that control a system and quantify the influence that each factor exerts on a reference variable (Lin S. J. et al., 2007). It is often applied in studies that have an insufficient sample size and uncertainty about whether the data is truly representative (Kayacan et al., 2010; Huang J., 2011). The basic idea behind GRA is to compute the strength of the relationship between variables by examining the degree of proximity for certain geometrical or the degree of correlation between curves (Deng, 1989). In this study, we employed GRA to quantify the influence of several factors on the soil salinity of the 94 samples from the Huqu area.

In GRA, the original data series are divided into two types of series: a reference series that will be compared with all other variables and one or more affecting series (one per variable that potentially affects the values in the reference series). The grey strength of the relationship is calculated to represent the relative proximity of two series. A discrete sequence of ranks can then be generated, with the ranks depending on the strengths of each factor's relationship to the reference series. If the strength of the relationship for one affecting series is higher than that of the others, the former series is considered to have a greater influence than the others on the reference series (Deng, 1989).

The first step in GRA is to generate the reference series and the affecting series. Since the range of values and the units of measurement in one data series may differ from those in other series, the original data are first normalized by dividing each value by the maximum value in the series, thereby producing a range of values from 0 to 1, and are then used to calculate the grey relational coefficient between the reference series and the affecting series (Sallehuddin R., et al., 2008). The reference series is represented as $x0(k) = x0(1), x0(2), \ldots x0(n)$, where k is the number of sample data, with $k \in (1, 2, \ldots, n)$, and n is the number of factors. Each affecting series is represented as $xi(k) = xi(1), xi(2), \ldots xi(n)$, where i represents the affecting series. In this study, we used the soil $EC_{1:5}$ (dS/m) as the reference series. Based on our review of the research literature and the mechanisms of salinization, as well as based on data availability, we selected six affecting factors for use as the affecting series (Table 3).

Table 3 Definitions of the affecting factors for the reference series (soil $EC_{1:5}$)

Affecting factor	Definition	Measurement
Xi (1)	Elevation of the sample site	Distance above mean sea level
Xi (2)	Distance to the nearest irrigation canal	The distance between the sample point and the nearest canal
Xi (3)	Compound topographic index (CTI)	Defined in section 2.3
Xi (4)	Vegetation cover	The % coverage of the soil by vegetation
Xi (5)	Groundwater level	Distance from the ground surface to the top of the groundwater table
Xi (6)	Groundwater salinity	Total dissolved salt content in the groundwater

The grey relational coefficient for two series, ζi(k), can be calculated as follows:

$$\zeta i\ (k) = (\Delta\min + \zeta\,\Delta\max) / (\Delta 0i(k) + \zeta\,\Delta\max) \qquad (2)$$

Where $\Delta 0i(k) = |x0(k) - xi(k)|$ is the absolute difference between the reference factor x0(k) and the corresponding affecting factor xi(k); ζ represents a grey parameter with a value between 0 and 1, and that is often assigned a value equaled 0.5, a value that is commonly used (Song, S., et al., 2011); and Δmin and Δmax represent the smallest and biggest values, respectively, among all of the Δ0i(k) affecting values.

The grey relational grade, γi, for the relationship between each affecting series xi(k) and the reference series x0(k) can be calculated by averaging the grey relational coefficient corresponding to each affecting factor:

$$\gamma i = (1/n)\ \Sigma[\zeta i(k)) \qquad (3)$$

The ranking of the affecting factors is then conducted based on the computed grey relational grades. As mentioned earlier, a higher value of the grey relational grade indicates a stronger relationship between the two series and suggests that the corresponding affecting factor is closer to the reference series than other affecting factors (Gao et al., 2013)

2.3 Results and discussions

2.3.1 Statistical description

Fig. 6 shows the frequency distribution and descriptive statistics for $EC_{1:5}$ of the cropland and other land types. 21 soil samples were collected from cropland during the spring, which explains why many samples have a low $EC_{1:5}$ value. 73 soil samples were collected from other land types (shrubland, abandoned land, sparse grassland and saline wasteland). Fig. 6 also shows wide variation in the $EC_{1:5}$ data, with values ranging from 0.11 to 23.1 dS/m (two orders of magnitude).

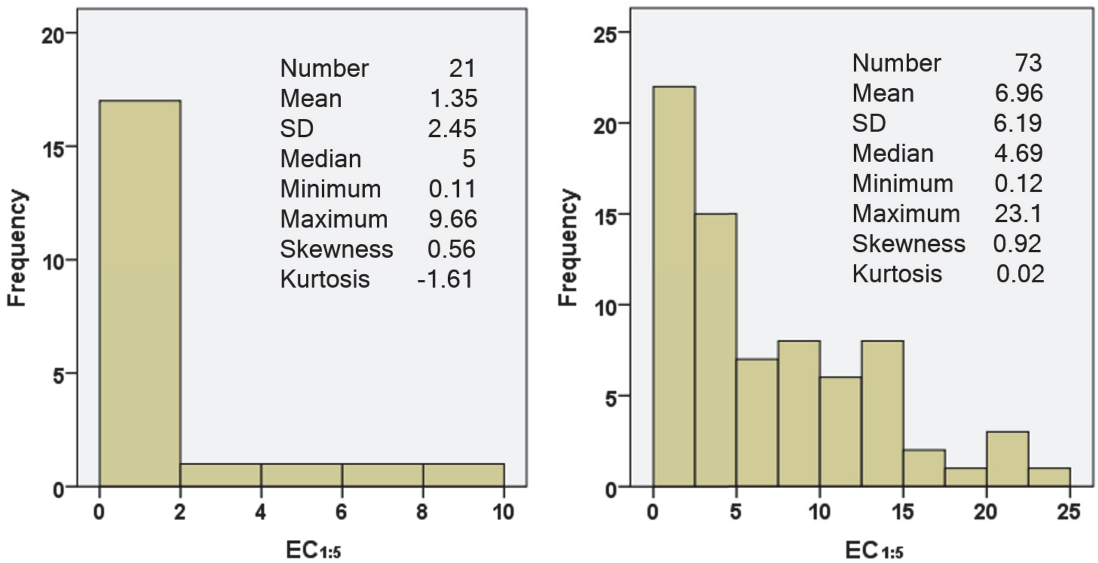

Fig. 6 Histograms of $EC_{1:5}$ values for samples from (a) cropland (n = 21) and (b) all other land types (n = 73), and their associated descriptive statistics

To understand the spatial distribution of the salinity levels, we mapped the distribution of soil $EC_{1:5}$ using ArcView based on equal interval method (Fig. 7). As the distribution map shows, most of the samples with high $EC_{1:5}$ were distributed at the margins of the oasis, but some were distributed in the center; in contrast, the samples with lower $EC_{1:5}$ were distributed throughout the oasis.

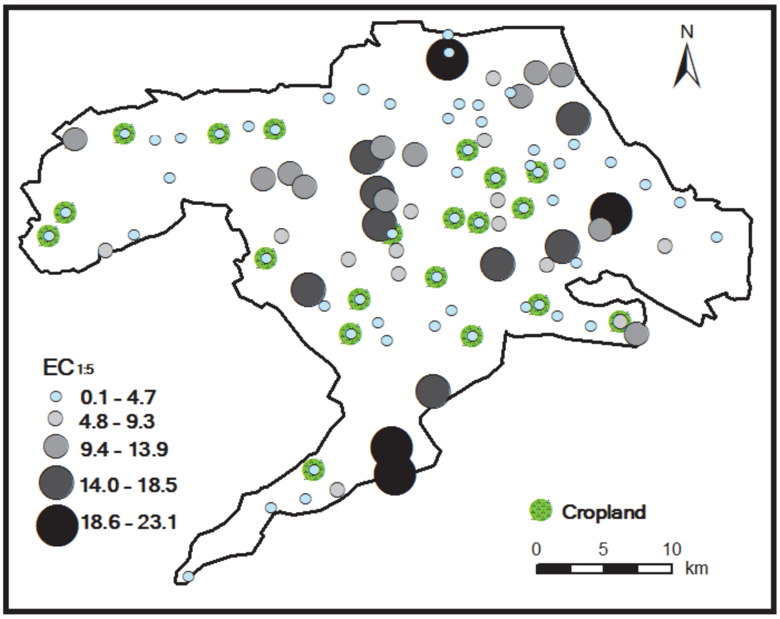

Fig. 7 Map of the distribution of $EC_{1:5}$ values for the 94 soil samples.

2.3.2 Differences in soil salinity among the different land use and cover types

To further explore the characteristics of the distribution of the soil $EC_{1:5}$ values in the Huqu area in relation to the land management in the study area, we classified the 94 samples into the five main land use and cover types: cropland, shrubland, abandoned land, sparse grassland, and saline wasteland. Table 2 summarizes the measured values of the various properties of the soil samples.

The coefficient of variation (CV) is the ratio of the standard deviation to the mean, and is often used as a general index of variability among the samples (Wilding and Drees, 1983). A CV value lower than 0.1 (10%) indicates low variability, whereas a CV value higher than 1.0 (100%) indicates high variability; intermediate values have moderate variability (Adhikari et. al, 2011). Table 4 shows that the CV values of $EC_{1:5}$ for cropland and shrubland were highly variable, with CV values greater than 1.0, which suggests that $EC_{1:5}$ and its distribution pattern are strongly influenced by human driving factors such as irrigation and farming activities as well as by the irrigation canal system. Despite regular irrigation, some of the cropland soil $EC_{1:5}$ values reached 9.66 dS/m, which indicates the existence of a secondary salinization problem. The shrubland is mainly artificial, and has resulted from a local policy to replace cropland with shrubs to combat desertification. The low soil moisture content of the shrubland provides evidence of a water scarcity problem. This is consistent with previous research, which showed that shrubs have died in large areas because the groundwater level fell below the level their roots can reach. The maximum $EC_{1:5}$ value of shrubland reached 14.89 dS/m, which indicated large amounts of salt accumulation in the topsoil as a result of a high evaporation rate combined with low rainfall and mineralization of the groundwater.

The CV values of $EC_{1:5}$ for abandoned land, sparse grassland, and saline wasteland were moderate (between 0.1 and 1.0). These land use and cover types were less strongly affected by human activities. Abandoned land was defined as land that had been abandoned for 5 to 20 years, and sparse grassland has been abandoned for more than 20 years and has begun to develop a grassland ecosystem. The majority of the soil $EC_{1:5}$ values for abandoned land were lower than those for sparse grassland, which indicated that soil salinity increased with increasing duration of abandonment. Compared with sparse grassland, the salinity level and moisture content of soils in the abandoned land were lower.

The CV values for SMC for all land use and cover types showed moderate variability (0.1 to 1.0). The $pH_{1:1}$ of the soil of the study areas ranged from 7.82 to 8.99 (slightly alkaline), and its low CV values (<0.1) indicated slight variation. The mean pH1:1 for all land use and cover types was greater than 8, which indicated most of the soil samples are weakly alkaline. The high groundwater salinity (>11 g/L) content and deep groundwater table depth (>15 m) indicated poor water quality and poor access to water, and their low CV values indicate moderate spatial variability.

Table 4 Descriptive statistics for the soil parameters, by land use and cover class (LUCC)a

LUCC (sample size)	Parameters	Range	Mean	SD	CV	LUCC description
Cropland (21)	$EC_{1:5}$ (dS/m)	0.11-9.66	1.35	2.39	1.77	This class includes land covered with crops (e.g., fennel, cotton, alfalfa, wheat, maize, sunflower, goji berry), newly cultivated land, and fallow land.
	$pH_{1:1}$	7.82-8.76	8.32	0.24	0.03	
	SMC (%)	0.86-13.81	7.15	2.77	0.39	
	GW salinity (g/L)	2.11-27.39	14.59	6.09	0.42	
	GW table depth (m)	5.32-32.33	18.61	7.99	0.43	
Shrubland (9)	$EC_{1:5}$ (dS/m)	0.12-14.89	3.23	4.45	1.38	Land with woody vegetation, with a total shrub cover that exceeds 10% of the surface. Some of this land resulted from a local policy of replacing cropland with shrubs to combat desertification.
	$pH_{1:1}$	8.05-8.99	8.38	0.31	0.04	
	SMC (%)	1.47-6.03	3.19	1.61	0.50	
	GW salinity (g/L)	9.68- 27.91	15.53	6.38	0.41	
	GW table depth (m)	7.17-29.95	18.47	8.34	0.45	
Abandoned land (5)	$EC_{1:5}$ (dS/m)	0.21-1.41	0.99	0.41	0.42	Land has been abandoned for 5 to 20 years, with vegetation cover <5%.
	$pH_{1:1}$	7.96-8.83	8.35	0.3	0.04	
	SMC (%)	1.54-4.55	2.66	1.07	0.40	
	GW salinity (g/L)	10.06-18.44	13.22	3.45	0.26	
	GW table depth (m)	10.89-28.78	20.05	6.66	0.33	
Sparse grassland (46)	$EC_{1:5}$ (dS/m)	0.15-21.44	6.18	5.01	0.81	Land has been abandoned for more than 20 years. Dominated by grasses and salt-tolerant grasses, with vegetation cover of 5% to 20%.
	$pH_{1:1}$	7.89-8.75	8.34	0.22	0.03	
	SMC (%)	0.93-10.18	4.08	2.14	0.52	
	GW salinity (g/L)	6.51-23.27	14.12	4.19	0.30	
	GW table depth (m)	7.18-36.05	22.70	6.33	0.28	
Saline wasteland (13)	$EC_{1:5}$ (dS/m)	8.28-23.10	14.6	5.12	0.35	Land with a salt crust at the soil surface. Dominated by natural salt-tolerant grasses, with vegetation cover >20%. Naturally salt-affected areas are distributed at the margins of the oasis.
	$pH_{1:1}$	7.88-8.58	8.36	0.22	0.03	
	SMC (%)	3.91-14.96	8.87	3.09	0.35	
	GW salinity (g/L)	7.55-19.97	11.20	3.39	0.30	
	GW table depth (m)	6.76-29.42	15.80	8.29	0.52	

[a] SMC represents the soil moisture content as a percentage of the dry soil weight. GW represents the groundwater.

2.3.3 Casual factors

Many factors, including soil factors, hydrological factors, management factors, and other factors, affected the soil salinization process and its spatial distribution in the Huqu area. Interactions among these factors are complex (Aslam et al., 2006). Based on the calculated value of the grey relational grade (γ), we determined the order of each affecting factor for all 94 samples combined. As shown in Table 3, these values range from 0 to 1, and we obtained the following ranking of the factors based on the grey relational grades: distance to the nearest irrigation canal > groundwater salinity > CTI > elevation of the sample site > groundwater level > vegetation cover.

Table 5 Grey relational grade (γ) and the resulting ranking for each affecting factor

Reference factor	Affecting factor	Definition	γ	Ranking	Relationship [a]
X_0 $EC_{1:5}$	X_i (2)	Distance to irrigation canals	0.814	1	Positive
	X_i (6)	Groundwater salinity	0.810	2	Negative
	X_i (3)	*CTI*	0.804	3	Positive
	X_i (1)	Elevation of the sample site	0.801	4	Negative
	X_i (5)	Groundwater level	0.798	5	Negative
	X_i (4)	Vegetation cover	0.771	6	Negative

[a] Positive relationships mean that a high value of the affecting factor increased $EC_{1:5}$; negative relationships mean that a high value decreased $EC_{1:5}$

Analyzing the grey relationships between the affecting factors and soil $EC_{1:5}$ for specific land use and cover types will help us to better understand the interaction between these factors and the salinization processes. To do this, we selected the two main land use and cover types and applied GRA to their affecting factors (Table 4).

Table 6 Grey relational grade (γ) for each affecting factor and the resulting ranking for the two main land use and cover types

Reference factor	Affecting factor	Definition	γ	Ranking	Relationship [a]
Cropland					
X_0 $EC_{1:5}$	X_i (2)	Distance to irrigation canals	0.847	1	Positive
	X_i (5)	Groundwater level	0.787	2	Negative
	X_i (3)	*CTI*	0.783	3	Positive
	X_i (1)	Elevation of the sample site	0.780	4	Negative
	X_i (6)	Groundwater salinity	0.777	5	Positive
	X_i (4)	Vegetation cover	0.760	6	Negative
Sparse grassland					
Reference factor	Affecting factor	Definition	γ	Ranking	Relationship [a]
X_0 $EC_{1:5}$	X_i (6)	Groundwater salinity	0.755	1	Positive
	X_i (4)	Vegetation cover	0.742	2	Positive
	X_i (1)	Elevation of the sample site	0.714	3	Negative
	X_i (5)	Groundwater level	0.711	4	Positive
	X_i (3)	*CTI*	0.708	5	Negative
	X_i (2)	Distance to irrigation canals	0.662	6	Negative

[a] Positive relationships mean that a high value of the affecting factor increased $EC_{1:5}$; negative relationships mean that a high value decreased $EC_{1:5}$.

Table 6 shows the calculated grey relational grades for the affecting factors for cropland and sparse grassland. For the cropland soil samples, the distance to the nearest irrigation canals was the most important factor for soil $EC_{1:5}$, and had a positive relationship with soil $EC_{1:5}$. The greater the distance between the sample sites and the canal, the higher the soil $EC_{1:5}$ content. This is because the use of fresh river water as an irrigation source, coupled with the drainage system, greatly, decreased salt accumulation in the topsoil. In contrast, the groundwater salinity had a negative relationship with soil $EC_{1:5}$, which was mainly because farmers combined fresh river water with groundwater to irrigate the croplands. The higher the groundwater salinity, the less of it can be used for irrigation and the more river water must be consumed for irrigation, leading to accelerated salt leaching and reducing the salt accumulation in the soil. Some samples were taken from the margins of the oasis, where the groundwater salinity was strongly affected by highly saline desert groundwater. In addition, the groundwater table depth was at least 5.3 m (Table 3) in those areas with high groundwater salinity. Because this large distance interrupts the capillary rise of water from the groundwater table to the soil surface, salt movement from the groundwater into the topsoil was reduced (Solomon et al., 2015). The vegetation cover had the weakest impact on the soil $EC_{1:5}$ of cropland, mainly because little vegetation had developed at the beginning of the growing season, when we obtained our soil samples.

For sparse grassland, distance to the nearest canal was the weakest affecting factor. This was mainly because the sparse grassland was close to a natural condition because of low intervention by human activities (i.e., after abandonment for more than 20 years). The groundwater salinity had a strong positive relationship with soil $EC_{1:5}$ for sparse grassland, which indicated that local-scale hydrological factors affected the distribution and variation of surface soil salinity. The sparse grassland had been abandoned for more than 20 years, and most of the sparse grassland had suffered from secondary salinization. Some of the land has been abandoned for more than 40 years; severe adverse effects of intensive agricultural practices during the 1950s and 1960s made the land unsuitable for cultivation. Excessive groundwater extraction for irrigation caused a rapid deepening of the groundwater table and mineralization of the groundwater. The use of groundwater with a high salt content, coupled with strong evaporation, accelerated salt accumulation in the topsoil. This caused rapid degradation of productive land and, eventually, abandonment of this land. The soil $EC_{1:5}$ values in this land could reach as high as the values in saline wasteland. The vegetation cover was the second-strongest affecting factor due to dense growth of halophytes in salt-affected areas (Chang Z. et al., 2007).

2.4 Conclusions

Salt-affected soils were distributed throughout the Huqu area. Most of the cropland had relatively low soil salinity, but several samples had high $EC_{1:5}$, which indicates a high potential for secondary salinization. The saline wasteland had some of the highest salinity values, and was concentrated mainly at the margin of the oasis, where there was no irrigation. Secondary salinized land was mainly located in areas of sparse grassland inside the oasis. The CV values of soil $EC_{1:5}$ for cropland and shrubland were greater than 1.0, which indicates that soil $EC_{1:5}$ and its distribution were strongly influenced by human activities.

Land-use practices also strongly influenced the distribution of salt-affected soils. The abandoned cropland had low salinity, but the long-abandoned cropland (which became sparse grassland) tended to have high salinity, sometimes reaching values as high as those in saline wasteland. In addition, transforming cropland to shrubland could result in further land degradation in Huqu area; due to the water scarcity and poor water quality, this change led to higher $EC_{1:5}$ and lower SMC. Improved management should focus on these lands to prevent further degradation.

The distance to the nearest irrigation canal was the most important factor for determining the salinity of cropland. The access to fresh river water and good drainage, combined with a deep groundwater table, prevented salt accumulation in the topsoil. However, the use of highly saline water and improper drainage and soil management will increase the risk of secondary salinization in irrigated soils. Therefore, proper irrigation methods, an improved drainage system, and effective soil management will be necessary to prevent non-salinized cropland from undergoing secondary salinization and to remediate existing salinized cropland.

The small sample size in this study may have made the data less reliable. However, the use of GRA should have mitigated this problem. Nonetheless, obtaining more and better data on water and soil properties would improve the ability to support management of the water and soil resources of the Minqin oasis, particularly if combined with remote sensing and GIS techniques to improve our ability to detect the distribution of salt-affected soils over larger areas.

Chapter 3 Derivation of salt content in salinized soil from lab-hyperspectral reflectance data

Chapter 3 Derivation of salt content in salinized soil from lab-hyperspectral reflectance data

3.1 Objectives

The aim of this study was to integrate laboratory-derived hyperspectral data with measured concentrations of salt in soil to develop a linear model for predicting soil salinity from hyperspectral data. We developed and used a normalized difference spectral index of salinity that integrates any two randomly selected hyperspectral wavebands to obtain all possible waveband pairs. Then, we used correlation of the indexes obtained for all of the possible waveband pairs with the wavebands corresponding to measured soil salinities to identify the pair of wavebands that showed the greatest sensitivity to the dominant salts in the soil. Finally, we applied linear regression analysis to derive a quantitative model for estimation of salt concentration from hyperspectral data

3.2 Materials and methods

3.2.1 Soil sampling and laboratory analysis

Our field work was conducted in Huqu region in 2015, during April, when salt concentrations in surface soils reach their annual maxima owing to the lack of rainfall and strong evaporation at that time of year. Samples were collected from the upper soil layer (0–10 cm depth) at 64 sites (Fig. 7). At each sampling site, we collected soil at five randomly selected locations within a 30 m × 30 m square and combined the five samples in the laboratory to represent the soil within that area. To determine the coordinates of the samples we used a handheld GPS receiver (MAP64SJZ, Garmin Ltd., Longmont, CO, USA).

The samples were taken to the Key Laboratory of Desert and Desertification at the Northwest Institute of Eco-Environment and Resources (Lanzhou city, China) for chemical analysis and spectral reflectance measurement. Samples were air-dried, ground, and sieved (1-mm mesh) to remove large particles and plant residues. They were then analysed for electrical conductivity, pH, organic matter content (OMC), and soluble salt content (Na+, K^+, Ca^{2+}, Mg^{2+}, Cl^-, SO_4^{2-}, CO_3^{2-}, HCO_3^-). Electrical conductivity (EC) and soil pH were measured in deionized distilled water at soil:water ratios of 1:5 g/ml and 1:1 g/ml, respectively (Thomas et al., 1996). The amounts of Na^+, K^+, Ca^{2+}, Mg^{2+}, Cl^- and SO_4^{2-} in samples were measured using an ion chromatograph (Dionex ICS-900, Thermo Fisher Scientific Inc., Waltham, USA). Amounts of CO_3^{2-} and HCO_3^- were measured using the double indicator titration method. The total soluble salt content (SSC) of each sample was determined on the basis of the total mass of the eight ionic concentrations determined (Bao, 2000). To measure organic carbon content (OCC), the soil samples were further sieved to isolate the < 0.1 mm size fraction.

To determine the spectral characteristics of different levels of soil salinity, the spectra of the 64 soil samples were divided into five salinity ranges as follows: 8 samples with $4 < SSC \leq 10$ g/kg, 14 samples with $10 < SSC \leq 20$ g/kg, 9 samples with $20 < SSC \leq 30$ g/kg, 19 samples with $30 < SSC \leq 39$ g/kg, and 14 samples with $39 < SSC \leq 51$ g/kg.

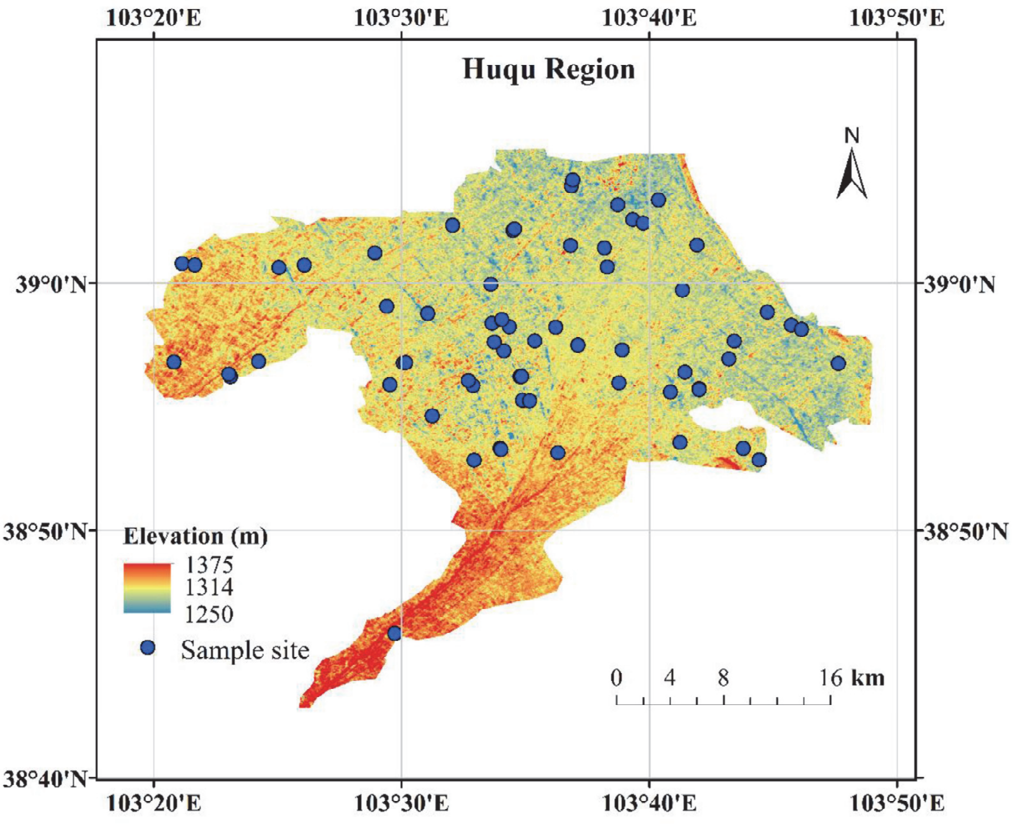

Fig. 8 Topographic map of the study area showing locations of 64 soil sampling sites.

3.2.2 Measurement of spectral reflectance in laboratory

To ensure stable atmospheric and uniform illumination conditions, spectral measurements were conducted in a dark room with one halogen lamp (Lowel Light Pro, JCV 14.5V-70WC) illuminating the sample from a nadir position 20 cm above the sample surface such that the target filled the field of view of the spectrometer (Zhang et al., 2014). We used a spectroradiometer (FieldSpec 4, Analytical Spectral Devices Inc., Longmont, USA) to acquire reflectance spectra of the soil samples at wavelengths between 350 and 2500 nm. The spectroradiometer uses individual detector arrays to record spectra at VNIR (350–1050 nm), SWIR1 (1000–1800 nm) and SWIR2 (1800–2500 nm) wavelengths. Sampling intervals were 1.4 nm for wavelengths 350–1000 nm (spectral resolution 3 nm) and 2 nm for wavelengths 1000–2500 nm (spectral resolution 10 nm); thus, spectral resolution varied from 3 nm for the very short wavelengths to 10 nm for the longest wavelengths (Danner et al., 2015).

Reflectance data were collected by using a fibre optic probe with a 25° field of view that was installed on a tripod about 30 cm above the target and at about 15° off nadir, which provided an observed surface area of 177 cm^2. Each soil sample was filled to overflowing in a Petri dish (10 cm diameter, 1 cm thick) and the upper surface was scraped off to provide a flat surface (Zhang, 2014). To minimize instrument noise we used the mean of 20 measured spectra for each soil sample. Before each measurement, reflectance was calibrated against a white reference panel of known reflectance (LapSphere Spectralon Diffuse Reflectance Panel) (Farifteh et al., 2008).

3.2.3 Spectral data processing

Sensory errors inherent in the Analytical Spectral Devices (ASD) spectroradiometer caused gaps in the signal at wavelengths of 1000 and 1800 nm, between the domains of the three detector arrays. These errors were corrected by applying the ASD ViewSpecPro program to smooth the “splices” between detector array domains (Danner et al., 2015).

To enhance small absorption features and better discriminate subtle differences in spectral features among samples, a continuum-removal (CR) algorithm (ENVI image processing package, Research Systems Inc., Boulder, USA) was applied to all of the saline soil spectra we measured. The continuum is a convex "hull" of line segments fitted along the top of a spectrum curve to connect local spectral maxima and represents the baseline against which other, more subtle absorption features are evident (Clark and Roush, 1984; Huang et al., 2004; Farifteh et al., 2008). To remove continuums for each waveband, the reflectance value at each point in an absorption feature was divided by the reflectance level of the corresponding convex hull; the resulting ratio is known as CR-reflectance (Huang et al., 2004). We also determined a mean spectrum of CR-reflectance to represent the basic spectral characteristics of the five ranges of soil salinity defined in section 2.2.

3.2.4 Selection of sensitive bands

We developed a normalized difference spectral index (NDSI, Eq. 2) to predict soil salinity from CR-reflectance data.

$$NDSIi,j,n = (CRRi,n - CRRj,n) / (CRRi,n + CRRj,n), \tag{2}$$

where n is the number of soil samples and CRR is the CR-reflectance of sample n for arbitrary wavebands i and j.

The NDSI, composed of two arbitrary waveband components in the 350–2500 nm (2151 wavebands in total) wavelength range, provided 2,312,325 candidate pairs for our 64 samples. Using one pair of waveband, 64 samples obtained 64 NDSI. Then the correlation analysis (Eq. 3) was applied to the NDSI and SSC for 64 samples. Likewise,we used correlation analysis to evaluate the relationships between the candidate NDSI waveband pairs and the known SSCs of 64 soil samples.

$$r = \frac{\sum_{i=1}^{n}(NDSI_{i,j}-\overline{NDSI_{\imath,\jmath}})(SSC_i-\overline{SSC})}{\sqrt{\sum_{i=1}^{n}(NDSI_{i,j}-\overline{NDSI_{\imath,\jmath}})^2\sum_{i=1}^{n}(SSC_i-\overline{SSC})^2}}, \tag{3}$$

where r is the correlation coefficient between NDSI and SSC, n is the number of soil samples, $NDSI_{i,j}$ is the CR-reflectance of the spectrum for the jth band of the ith sample, SSC_i is the soluble salt content of the ith sample, and $\overline{NDSI\imath,\jmath}$ and $\overline{SSC}$ are the means of NDSI and soluble salt content, respectively.

The correlation coefficients (r) between SSC values and all possible candidate NDSIs were used to evaluate the contribution of NDSI to the estimation of soil salinity. The pair of bands with highest correlation coefficient were taken to be the pair with greatest sensitivity to soil salinity.

3.2.5 Retrieval modeling

Among the 64 soil samples, thirty-three samples were used to attempt to establish a linear model of the relationship between NDSI and SSC by univariate regression with measured SSCs as the dependent variable and NDSI as the independent variable. The measured SSCs of the remaining 31 samples were used to validate the model.

3.3 Results and discussions

3.3.1 Descriptive statistics of chemical properties of soils

Descriptive statistics on the chemical properties of the 64 soil samples we collected are provided in Table 1. The soil samples showed a broad range of salinity from 4.07 to 51.26 g/kg (median 31.54 g/kg). The predominant anions in the samples were SO_4^{2-} and Cl^- and the predominant cations were Na^+ and Ca^{2+}.

The correlation coefficient between SO_4^{2-} and Na^+ was 0.295, that between Cl^- and Na^+ was 0.800, and that between Cl^- and Ca^{2+} was 0.789 (Table 8). There were also strong correlations of SSC with Ca^{2+} (r = 0.854), Cl^- (r = 0.695) and SO_4^{2-} (r = 0.587). Thus, it is likely that most of the chemical compounds in the soil samples are chlorine and sulphate compounds.

Although both K^+ and Mg^{2+} showed strong positive relationships with Cl^- and SSC, which might indicate the presence of KCl or $MgCl_2$, their very low mean concentrations (0.15 and 0.29 g/kg for K^+ and Mg^{2+}, respectively) indicate that KCl and $MgCl_2$ were not dominant salts in the soil samples.

There were very low contents of HCO_3^- in the soil samples and no CO_3^{2-} was identified, which together indicate that there was little in the way of bicarbonate compounds and no discernible carbonate compounds in the soils.

Table 7 Descriptive statistics of chemical properties of 64 soil samples

	Na^+ g/kg	K^+ g/kg	Mg^{2+} g/kg	Ca^{2+} g/kg	Cl^- g/kg	SO_4^{2-} g/kg	HCO_3^- g/kg	CO_3^{2-} g/kg	$EC_{1:5}$ mS/cm	SSC g/kg	OCC g/kg
Max	20.84	0.51	2.07	4.76	17.80	40.56	0.34	0	22.36	51.26	7.36
Min	0.00	0.03	0.01	0.05	0.68	2.37	0.01	0	0.14	4.07	2.22
Mean	4.13	0.15	0.29	2.11	5.70	15.50	0.14	0	5.59	28.01	4.83
SD	5.50	0.12	0.37	1.56	4.28	9.60	0.05	0	5.61	13.34	1.16
CV	1.33	0.77	1.30	0.74	0.75	0.62	0.39	0	1.00	0.48	0.24

* SD, standard derivation; CV, coefficient of variance (ratio of standard derivation to the mean).

Table 8 Correlation matrix of relationships between variables

	Na^+	K^+	Mg^{2+}	Ca^{2+}	Cl^-	SO_4^{2-}	HCO^{3-}	$EC_{1:5}$	SSC
Na^+	1								
K^+	0.815**	1							
Mg^{2+}	0.668**	0.550**	1						
Ca^{2+}	0.782**	0.759**	0.661**	1					
Cl^-	0.800**	0.724**	0.718**	0.789**	1				
SO_4^{2-}	–0.285*	–0.108	–0.128	0.195	–0.100	1			
HCO^{3-}	–0.049	0.140	0.004	–0.006	0.110	–0.125	1		
$EC_{1:5}$	0.961**	0.795**	0.717**	0.806**	0.817**	–0.230	–0.062	1	
SSC	0.579**	0.601**	0.522**	0.854**	0.695**	0.587**	–0.074	0.611**	1

**Significant at 0.01 probability level (2-tailed). *Significant at 0.05 probability level (2-tailed)

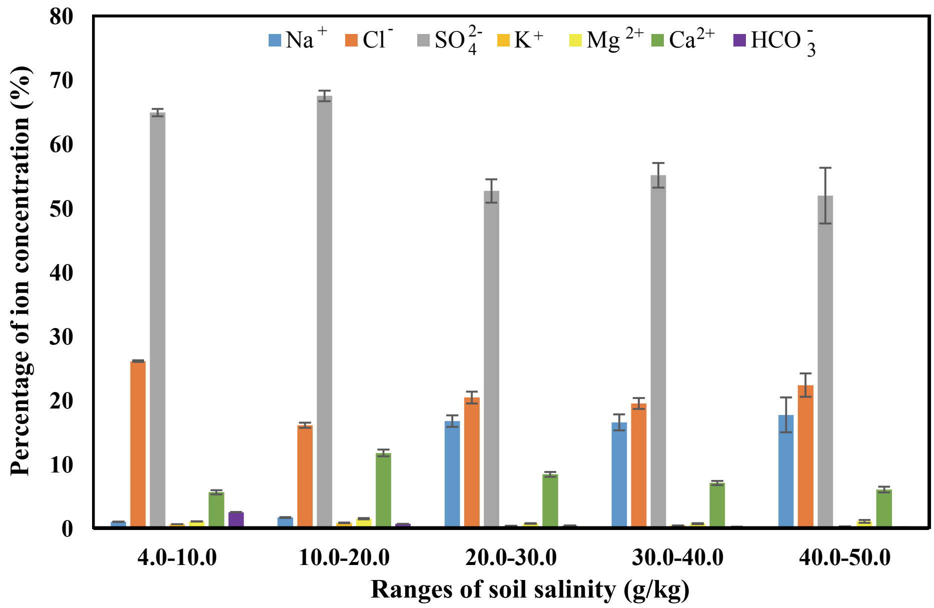

Fig. 9 Concentrations of Na^+, K^+, Ca^{2+}, Mg^{2+}, Cl^-, SO_4^{2-} and HCO_3^- ions in samples for each of the five ranges of soil salinity defined in section 2.2. The percentage concentration for each ion was calculated as its concentration divided by the total cation and anion concentration for that salinity range.

The dominant anions in each of the five salinity ranges were SO_4^{2-} and Cl^- (Fig. 8). The concentration of bicarbonate decreased with increasing soil salinity. As soil salinity increased, Na^+ became the dominant cation for ranges of $20 < SSC \leq 30$ g/kg, $30 < SSC \leq 39$ g/kg and $39 < SSC \leq 52$ g/kg. The concentrations of Ca^{2+} were relatively high for all salinity ranges, which indicates that the dominant salts were probably $CaSO_4$ and $CaCl_2$ for the lower salinity samples ($4 < SSC \leq 10$ g/kg and $10 < SSC \leq 20$ g/kg). For higher salinity ranges ($20 < SSC \leq 30$ g/kg, $30 < SSC \leq 39$ g/kg, $39 < SSC \leq 51$ g/kg), the dominant salts were probably NaCl, $CaSO_4$, $CaCl_2$ and $NaSO_4$. Concentrations of Ca^{2+} initially increased with increasing soil salinity up to 20 g/kg, but then decreased with further increases of salinity. The concentration of HCO_3^- decreased as soil salinity increased across the entire salinity range (Fig. 8).

3.3.2 Spectral features of soil samples

The spectra of all 64 samples were of similar shape with considerable overlap (Fig. 9-a). The representative spectra for the five ranges of salinity (Fig. 9-b) exhibited several differences in the width of reflectance peaks and depth of absorption troughs. CR-processing of the spectra strengthened the peaks and troughs of these spectra (Fig. 9-c and 9-d). The spectra for samples in each of the five salinity ranges showed similar absorption features at wavelengths of about 1400, 1900 and 2200 nm. These features are associated with the particular salts in the soils and are related to the internal vibrational processes of anions (e.g., OH^-, SO_4^{2-} and the Al-OH group) or to water molecules that are trapped in or adsorbed on the crystal structure (Hunt, 1977; Crowley, 1991). The internal vibrational processes of the anion groups were the result of overtones or combinations (stretching and bending modes) of fundamental vibrations and of vibrations of the entire lattice (Hunt and Salisbury, 1970; Hunt and Salisbury1971; Hunt et al., 1971[a]; Hunt et al., 1971[b]; Hunt et al., 1972; Hunt et al., 1976; Kahle, 1982; Goetz, 1989; Mougenot et al., 2009). The broad absorption features near 1400, 1940 and 2250 nm are probably related to fluid inclusions in halite (NaCl) after drying (Clark and Roush, 1984; Crowley, 1991; Danner et al., 2015). The features near 2200, 2300 and 2400 nm probably represent O–H stretch, or AlOH/MgOH bending mode, or the combined effect of both. Previous research has shown that these salt minerals (e.g., chlorine compounds) are the dominant evaporate minerals that form crystals or efflorescence in salinized crusts and scalds in arid and semi-arid regions (Farifteh et al., 2008). Moreover, previous researchers have suggested that absorption features at around 1000, 1200, 1400, 1600, 1740, 1900, 2200 and 2330 nm might also be affected by combination overtones of O–H stretching, H–O–H bending fundamentals, and various overtones in gypsum ($CaSO_4 \cdot 2H_2O$) (Howari et al., 2002).

In the region from 350 to 1000 nm, no marked differences were distinguishable among the spectra for the five salinity ranges (Fig. 10-c). At wavelengths higher than 1300 nm, salinity-induced changes in soil reflectance were evident, particularly in the water absorption bands at around 1400 and 1900 nm (Fig. 10-c). Reflectance for the lower salinity ranges were higher than those of the higher salinity ranges at about 1344–1619 nm (Fig. 10-d) and 2422–2488 nm (Fig. 10-f). In contrast, reflectance for the higher salinity ranges were higher than those of the lower salinity ranges near a small peak at 2241–2387 nm (Fig. 9-e). The depths of the absorption troughs centred at about 1410 and 1940 nm increased with increasing salinity.

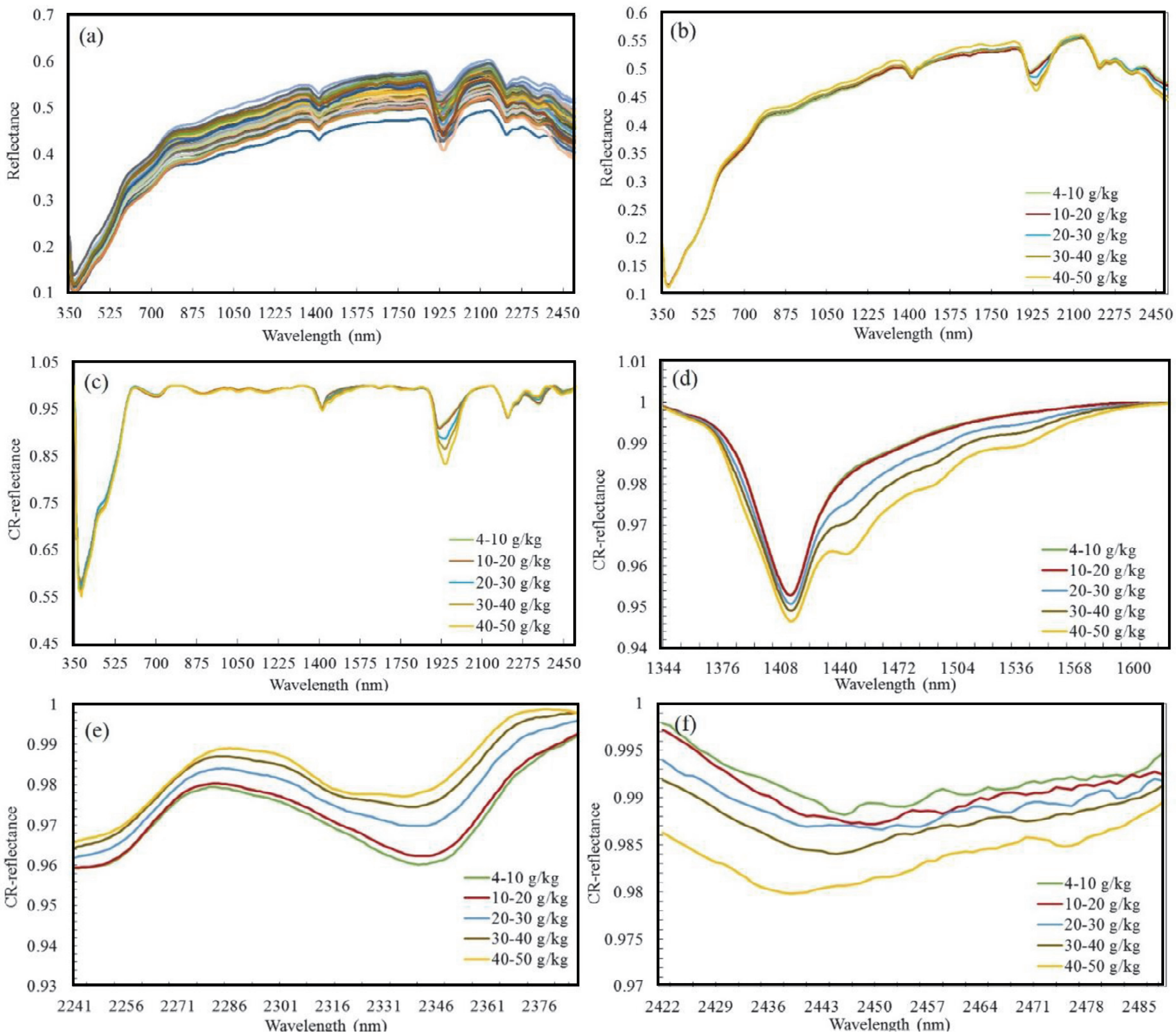

Fig. 10 Reflectance spectra: (a) original measured spectra of all 64 soil samples, (b) averaged spectra of samples in five salinity ranges, (c) CR-reflectance spectra of samples in five salinity ranges, (d) enlargement of panel for range of 1344–1619 nm, (e) enlargement of panel for range of 2241-2387 nm, (f) enlargement of panel for range of 2422–2488 nm.

3.3.3 Modeling of SSC and model validation

Correlation of the wavebands of measured salinities of 64 samples with all of the waveband pairs used in the NDSI (Fig. 10) produced strong correlations (absolute value of $r > 0.84$) for the following pairs: 750–920 nm and 2351–2487 nm, 1199–1379 nm and 2351–2487 nm, 1553–1765 nm and 2351–2487 nm, and 2118–2261 nm and 2351–2487 nm. The bands including wavelengths 1358 and 2382 nm ($r = -0.87$) were identified as the most promising bands to use to develop a quantitative model for estimation of salt concentration from hyperspectral data.

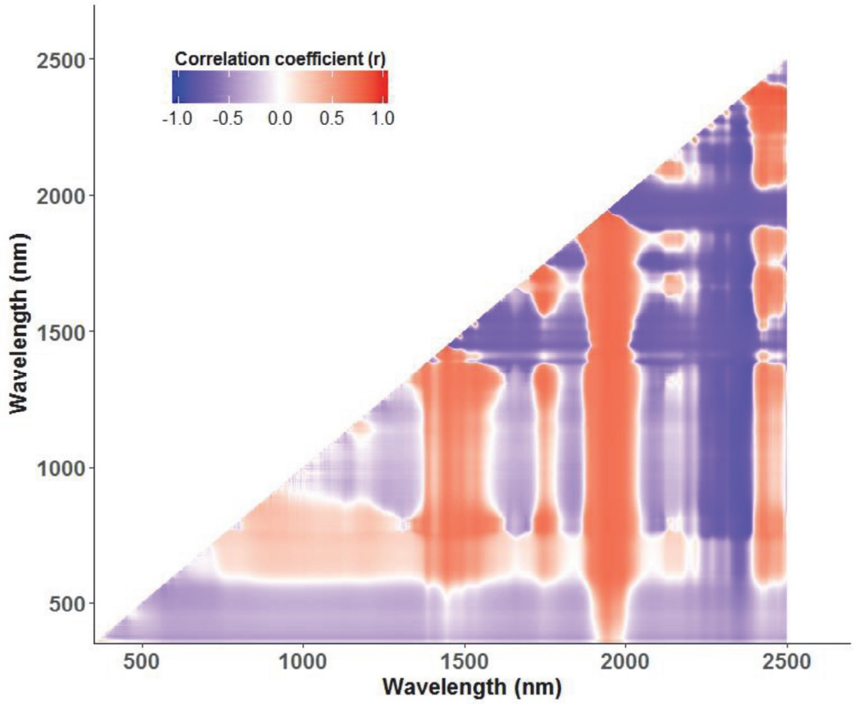

Fig. 11 Heatmap of correlation coefficients (r) for correlations of wavebands of measured salinities with all candidate NDSI waveband pairs

We therefore defined the following normalized difference spectral index (NDSI):

$$NDSI1 = (B2382 - B1358) / (B2382 + B1358), \quad (4)$$

where B1358 and B2382 are CR-reflectance of spectral bands at 1358 and 2382 nm, respectively.

The model we established by univariate linear regression to estimate SSC from hyperspectral data (Fig. 12-a) was:

$$SSC\ (g/kg) = 5312.3 \times NDSI1 + 34.187\ (R^2 = 0.8272) \quad (5)$$

Validation of the predicted values of SSC against measured values (Fig. 12-b) showed that Eq. 5 over-estimated SSC, which we attributed to the presence in our samples of some salt ions (e.g., Fe, Al) that were not measured during laboratory analysis.

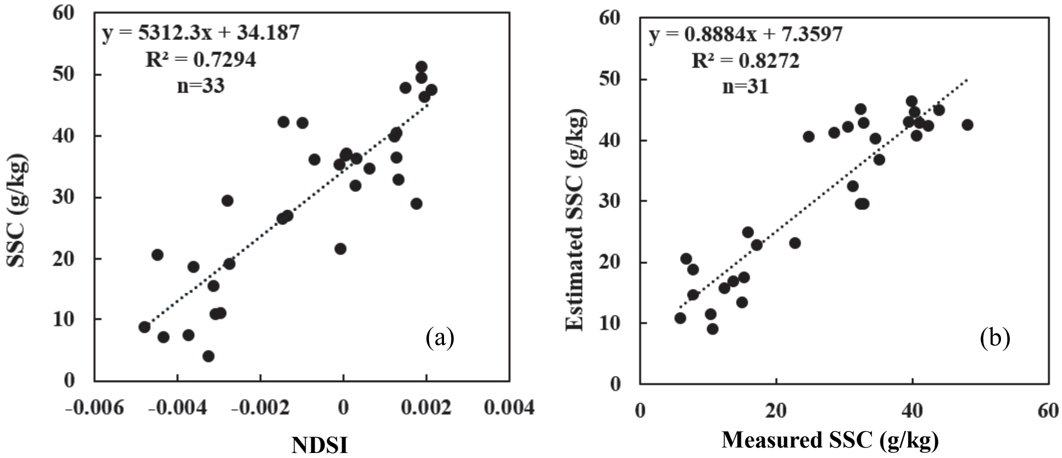

Fig. 12 (a) Measured soluble salt content (SSC) versus normalized difference spectral index (NDSI) and (b) scatter plot of measured SSC versus SSC estimated from Eq. 5

To ascertain which soluble salts the CR-reflectance wavelengths we selected were responsive to, we examined the relationships of ionic concentrations (Na^+, K^+, Ca^{2+}, Mg^{2+}, Cl^-, SO_4^{2-}, CO_3^{2-} and HCO_3^-) in our 64 samples with the CR-reflectance at 2382 and 1358 nm, and with our NDSI (Fig. 13). We found significant correlations between Na^+ and the CR-reflectance at 2382 nm ($r = 0.622$) and 1358 nm ($r = -0.603$), between Na^+ and NDSI ($r = 0.661$), between Cl^- and the CR-reflectance at 2382 nm ($r = 0.683$) and 1358 nm ($r = -0.561$), and between Na^+ and NDSI ($r = 0.711$). These results indicate that the two bands we used to construct an NDSI were best suited for soils where the dominant soluble salts contain chlorine and sulphate compounds. In contrast, in the Yellow River delta region of China, where the dominant soluble salts are NaCl and $MgCl_2$, CR-reflectance at 2052 and 2203 nm were used to construct a spectral soil salinity index (Weng et al., 2010). Moreover, in South Africa, where most of the salts in soils are of marine origin, reflectance at 2040 and 1410 nm were identified as the most promising for use in a spectral soil salinity index (Mashimbye, 2013). Thus, considering our results and those from other regions, it is evident that particular salts influence spectral reflectance differently, so the wavelengths employed in developing NDSIs should be selected on a case by case basis, although a particular NDSI may be applicable in areas with the same salt types as the area in which the NDSI was developed.

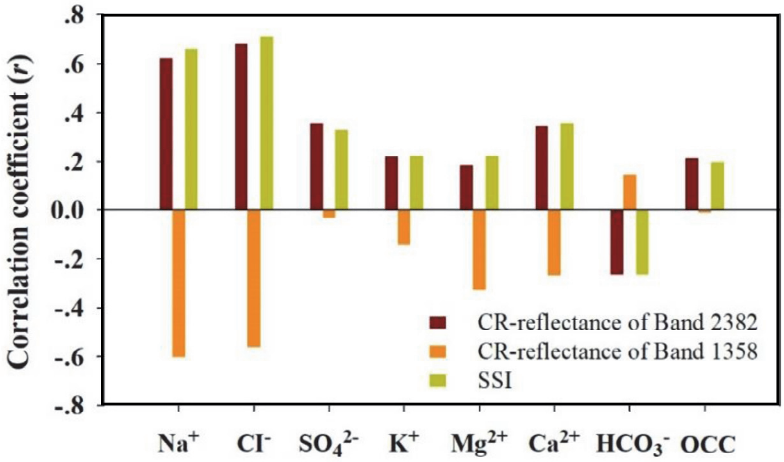

Fig. 13 Correlation coefficients (r) obtained for correlations of measured concentrations in our samples of seven ions and organic carbon content (OCC) with CR-reflectance at 2382 and 1358 nm, and with the NDSI we developed in this study. Correlations were significant at the 0.01 probability level except for correlations of CR-reflectance at 2392 nm with HCO_3^-, CR-reflectance at 1358 nm with Ca^{2+}, and NDSI with HCO_3^-, which were significant at the 0.05 probability level.

3.4 Conclusions

We collected 64 samples of surface soil in the Huqu region of Minqin oasis, an area in northwest China that has a severe soil salinization problem. Chemical analyses of the samples showed that the dominant salts were chlorine and sulphate compounds. We used a normalized difference spectral index of salinity that integrates any two randomly selected hyperspectral bands to obtain all possible waveband pairs that might be associated with the salts contributing to salinization. Correlation analysis of the indexes obtained for all of the possible waveband pairs with the corresponding measured soil salinities for all of the 64 samples showed that two bands centred at 2382 and 1358 nm were closely associated with sodium and chloride concentrations. We applied linear regression modelling to these bands to construct a spectral index. Validation of the index by correlation analysis of the index-derived salt content with measured salt content of 31 soil samples showed a strong correlation (R^2 = 0.8272). Thus, the model we derived successfully estimated the salt content of surface soils in the study area. Further research is needed on the application of this method to remotely sensed (aircraft or satellite) digital hyperspectral data so that its potential use for large-scale predictive mapping of the extent and severity of soil salinity can be investigated.

Chapter 4

Derivation of salt content in salinized soil from field-hyperspectral reflectance data

Chapter 4 Derivation of salt content in salinized soil from field-hyperspectral reflectance data

4.1Objectives

The aim of this study was to integrate field-derived hyperspectral data with measured concentrations of salt in soil to develop a linear model for predicting soil salinity from hyperspectral data. To do this, a normalized difference spectral index of salinity that integrates any two randomly selected hyperspectral wavebands will be developed and used to obtain all possible waveband pairs. Then, correlation of the indexes obtained for all of the possible waveband pairs with the wavebands corresponding to measured soil salinities to identify the pair of wavebands that have greatest sensitivity to the dominant salts in the soil. Finally, linear regression analysis will be applied to derive a quantitative model for estimation of salt concentration from field hyperspectral data

4.2 Materials and methods

4.2.1 Soil sampling and laboratory analysis

Our field work was conducted in Huqu region in 2015, during April, when salt concentrations in surface soils reach their annual maxima owing to the lack of rainfall and strong evaporation at that time of year. Samples were collected from the upper soil layer (0–10 cm depth) at 59 sites (Fig. 14). The sampling method and the laboratory chemical analysis of soil properties ($EC_{1:5}$, pH, OMC, Na^+, K^+, Ca^{2+}, Mg^{2+}, Cl^-, SO_4^{2-}, CO_3^{2-}, HCO_3^-) are same with chapter 3. The total soluble salt content (SSC) of each sample was the total mass of the eight ionic concentrations determined (Bao, 2000).

The spectra of the 59 soil samples were divided into five salinity ranges based on the standard used in previous chapter as follows: 8 samples with $4 < SSC \leq 10$ g/kg, 14 samples with $10 < SSC \leq 20$ g/kg, 9 samples with $20 < SSC \leq 30$ g/kg, 19 samples with $30 < SSC \leq 39$ g/kg, and 14 samples with $39 < SSC \leq 51$ g/kg.

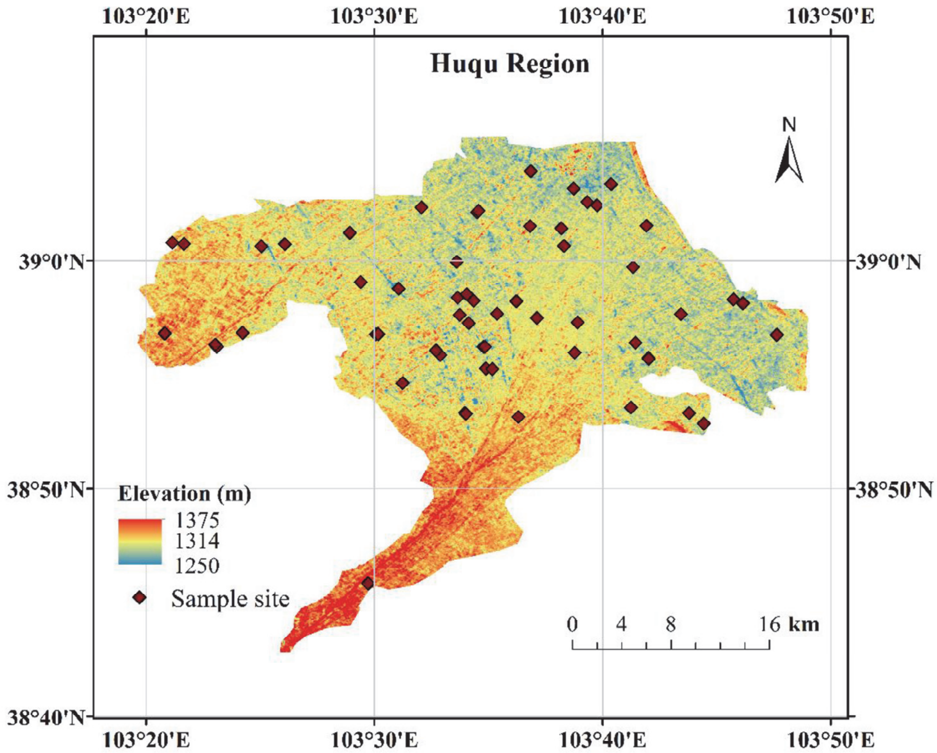

Fig. 14 Topographic map of the study area showing locations of 58 soil sampling sites.

4.2.2 Measurement of spectral reflectance in field and data processing

The field data set was obtained during the same time of soil sampling. Spectra data were collected by a FieldSpec HandHeld spectrometer, which has a spectral resolution of 3.3 nm on clear days between 11:00 am and 2:00 pm. Reflectance was calibration and optimization using a white panel of known reflectance (a barium sulfate panel). When detect surface features, the vertical range of spectrometer and the target is about 1.0 m. In order to minimize the noise of the reflectance spectral, we measured ten successive spectra at each of the sites and averaged them. We then chose the bands (400-1000 nm) with a relatively stable energy response and little noise to be used in analysis. In the meantime, 5 topsoil (0-5 cm) samples were gathered at each of the sites. The process of spectral data here was same with chapter 3.

4.2.3 Selection of sensitive bands

We used NDSI to predict soil salinity from CR-reflectance data. The NDSI, composed of two arbitrary waveband components in the 400–1000 nm (601 wavebands in total) wavelength range. Using one pair of waveband, 58 samples obtained 59 NDSI. Then the correlation analysis (Eq. 3) was applied to the NDSI and SSC for 58 samples. Likewise, we used correlation analysis to evaluate the relationships between the candidate NDSI waveband pairs and the known SSCs of 58 soil samples.

The correlation coefficients (r) between SSC values and all possible candidate NDSIs were used to evaluate the contribution of NDSI to the estimation of soil salinity. The pair of bands with highest correlation coefficient were taken to be the pair with greatest sensitivity to soil salinity.

4.2.4 Retrieval modeling

Among the 58 soil samples, thirty samples were used to attempt to establish a linear model of the relationship between NDSI and SSC by univariate regression with measured SSCs as the dependent variable and NDSI as the independent variable. The measured SSCs of the remaining 29 samples were used to validate the model.

4.2.5 Principal component analysis

Principal component analysis (PCA) is a well-known statistical technique, which has been used extensively to analyse large multidimensional datasets. PCA is used in multivariate correlation analysis (Boroson and Green, 1992). It is a mathematical tool used to describe the variance in the data set by the fewest number of variables called principal components (PCs). We applied principal component analysis to the CR-removed reflectance data of 401-999 nm. After the principal components were extracted, they will be used for regression analysis.

4.3 Results and discussions

4.3.1 Descriptive statistics of chemical properties of soils

Descriptive statistics on the chemical properties of the 58 soil samples we collected are provided in Table 9. The soil samples showed a broad range of salinity from 5.92 to

51.26 g/kg (median 31.54 g/kg).

Table 9 Descriptive statistics of chemical properties of 59 soil samples

	Na^+	K^+	Mg^{2+}	Ca^{2+}	Cl^-	SO_4^{2-}	HCO_3^-	CO_3^{2-}	$EC_{1:5}$	SSC	OCC
	g/kg	g/kg	g/kg	g/kg	g/kg	g/kg	g/kg	g/kg	mS/cm	g/kg	g/kg
Max	19.91	0.51	2.07	4.76	17.80	40.56	0.34	0	22.36	51.26	7.36
Min	0.00	0.03	0.01	0.05	0.68	3.62	0.01	0	0.14	5.92	2.22
Mean	4.04	0.15	0.29	2.14	5.81	15.78	0.14	0	5.27	28.34	4.74
SD	5.20	0.11	0.39	1.56	4.24	9.70	0.06	0	5.43	13.12	1.14
CV	1.29	0.74	1.31	0.73	0.73	0.61	0.41	0	1.03	0.46	0.24

* SD, standard derivation; CV, coefficient of variance (ratio of standard derivation to the mean).

Table 10 Correlation matrix of relationships between variables

	Na+	K^+	Mg^{2+}	Ca^{2+}	Cl^-	SO_4^{2-}	HCO^{3-}	$EC_{1:5}$	SSC
Na^+	1								
K^+	0.779**	1							
Mg^{2+}	0.727**	0.608**	1						
Ca^{2+}	0.777**	0.752**	0.678**	1					
Cl^-	0.785**	0.704**	0.743**	0.778**	1				
SO_4^{2-}	-0.298*	-0.100	-0.156	0.190	-0.099	1			
HCO^{3-}	-0.421**	-0.478**	-0.423**	-0.750**	-0.478**	-0.511**	1		
$EC_{1:5}$	0.983**	0.807**	0.797**	0.859**	0.834**	-0.193	-0.517**	1	
SSC	0.548**	0.576**	0.526**	0.842**	0.679**	0.604**	-0.800**	0.647**	1

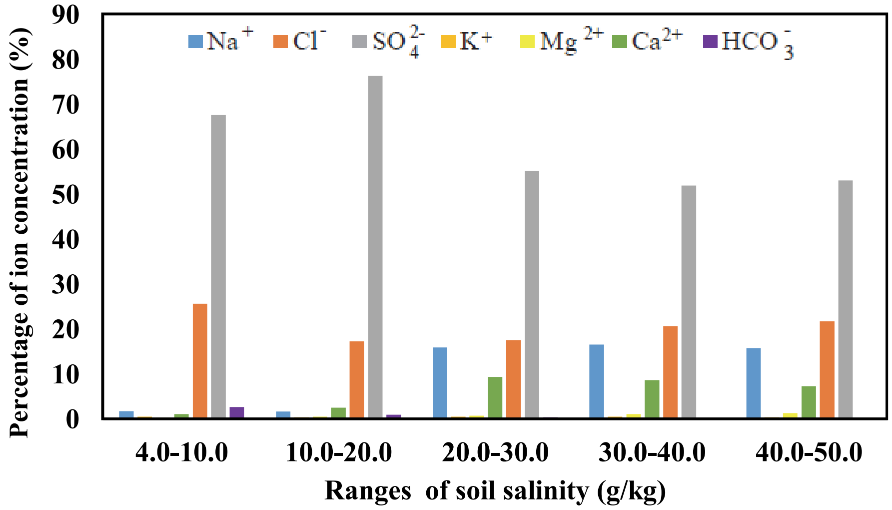

Fig. 15 Concentrations of Na^+, K^+, Ca^{2+}, Mg^{2+}, Cl^-, SO_4^{2-} and HCO_3^- ions in samples for each of the five ranges of soil salinity defined in section 2.2. The percentage concentration for each ion was calculated as its concentration divided by the total cation and anion concentration for that salinity range.

The dominant anions in each of the five salinity ranges were SO_4^{2-} and Cl^- (Fig. 15). The concentration of bicarbonate decreased with increasing soil salinity. Na^+ became the dominant cation for ranges of 20 < SSC ≤ 30 g/kg, 30 < SSC ≤ 39 g/kg and 39 < SSC ≤ 52 g/kg. The concentrations of Ca^{2+} were relatively high for all salinity ranges, which indicates that the dominant salts were probably $CaSO_4$ and $CaCl_2$ for the lower salinity samples (4 < SSC ≤ 10 g/kg and 10 < SSC ≤ 20 g/kg). For higher salinity ranges (20 < SSC ≤ 30 g/kg, 30 < SSC ≤ 39 g/kg, 39 < SSC ≤ 51 g/kg), the dominant salts were probably NaCl, $CaSO_4$, $CaCl_2$ and $NaSO_4$. Concentrations of Ca^{2+} initially increased with increasing soil salinity up to 20 g/kg, but then decreased with further increases of salinity. The concentration of HCO_3^- decreased as soil salinity increased across the entire salinity range (Fig. 15).

4.3.2 Modeling of SSC and model validation

4.3.2.1 Original spectrum

The spectrum (Fig.16-a) for 58 soil samples presented similar trends from wavelength 400-1000 nm. The correlation relationship analysis was applied to the original reflectance data and the SSC for 58 samples. There were negative relationship between them (Fig.16-b). The correlation relationship weaken at the range of 540-690 nm and then strengthen as the wavelength increased.

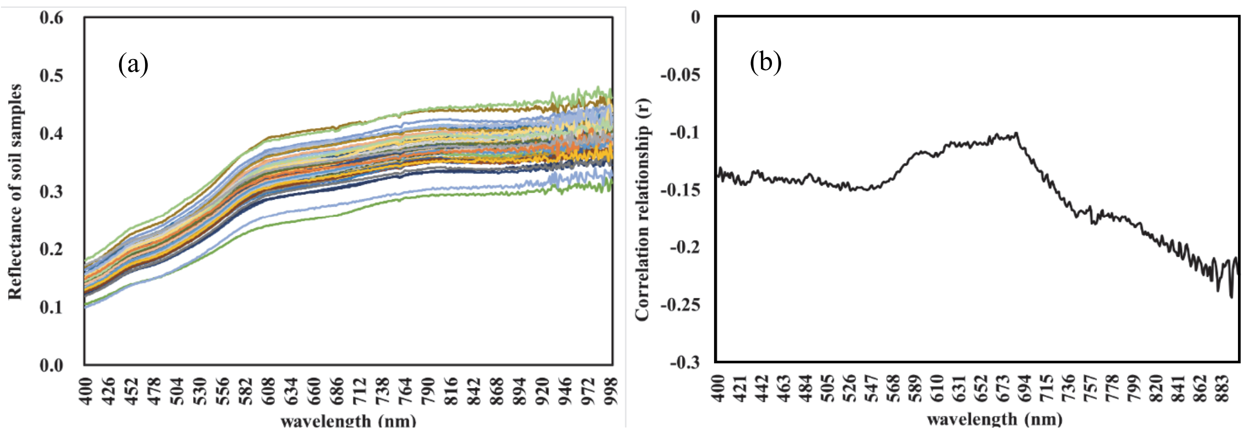

Fig. 16 (a) The spectrum of original reflectance for 58 soil samples (b) the correlation coefficient for original reflectance and SSC for 58 soil samples.

Two index in difference form (band1 – band 2) and NDSI form ((band1 – band 2)/

(band1 + band 2)) were used to detect the sensitive bands to SSC of soil samples. Optimal band combination that selected from the all of the waveband pairs were band 834 and band 836 for both difference and NDSI form (r = -0.47). Correlation heatmaps of the wavebands of measured salinities of 58 samples with all of the waveband pairs (Fig. 17) indicated that all the high correlated band pairs were the neighbour bands that are next to each other and ranging over all the wavelength, which indicated the difficulties to use original reflectance data to select sensitive bands to SSC.

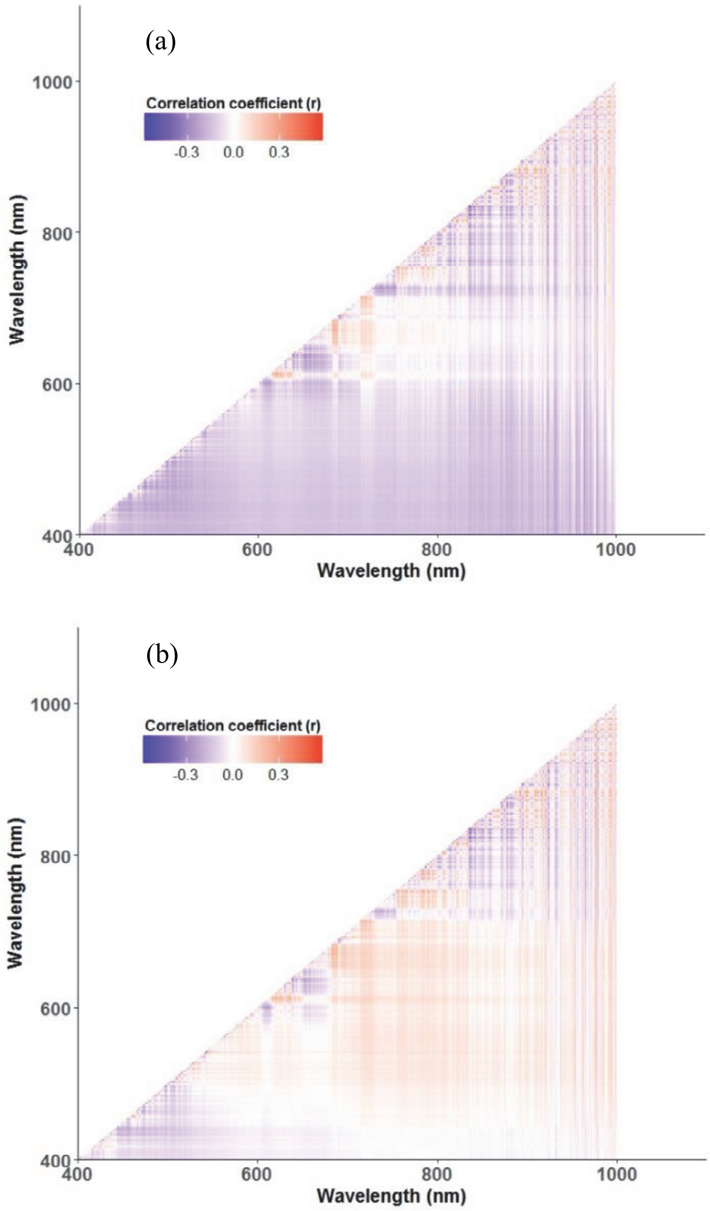

Fig. 17 (a) Heatmap of correlation coefficients (r) for measured salinities and all waveband pairs candidates from original reflectance data in difference form (b) heatmap of correlation coefficients (r) for measured salinities and all waveband pairs candidates from original reflectance data in NDSI form

4.3.2.2 First derivate spectrum based modeling and model validation

The derivative analysis of spectra reflectance was used primarily to eliminate the interference from changes in illumination or soil background. This approach is used to detect small peaks in the presence of baseline noise because small threshold setting results in the detection of noise and drift as parent analyse peaks. The first derivative is calculated for a wavelength intermediate between two wavelength and it emphasize sudden spectrum changes, for examples from a negative slope to a positive slope in the case of the red edge feature of vegetation reflectance spectrum. Such distinguishable features are especially useful for discriminating between peaks of overlapping bands (morry, 1968). The first derivative was calculated using a first difference transformation of the reflectance spectrum obtained from the polynomial fit. The first derivative was calculated using a first difference transformation of the reflectance spectrum (Dawson and Curran, 1998) as follows (Eqs. 6):

$$\frac{dR}{d\lambda} = \frac{R(\lambda_{i+1}) - R(\lambda_{i-1})}{\lambda_{i+1} - \lambda_{i-1}} \tag{6}$$

where $\frac{dR}{d\lambda}$ is the first derivative reflectance at a wavelength i, midpoint between wavebands i and $i+1$., $R\lambda_{(i+1)}$ is the reflectance at the $i+1$ waveband, $R\lambda_{(i-1)}$ is the reflectance at the i-1 waveband, and $\Delta\lambda$ is the difference in wavelengths between i and $i+1$.

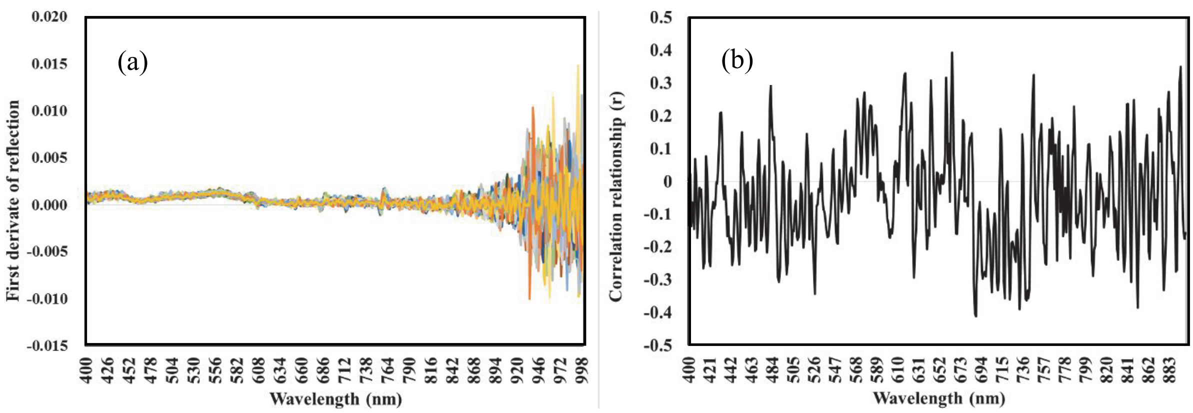

Fig. 18 (a) the spectrum of first derivate of reflectance for 58 soil samples (b) the correlation coefficient for first derivate values of spectrum and SSC for 58 soil samples.

The first derivate spectrum have low reflectance values at band range 400-800 nm and have high variation in values in the range of 800-1000nm. The correlation coefficient for first derivate values of spectrum and SSC has high variation and change from negative to positive values. The strongest negative coefficient was in the band of 689 with a value of -0.413 ($p > 0.05$) and strongest positive value in the band of 665 with a value of 0.392 ($p > 0.05$).

Two index in difference form (band1 – band 2) and NDSI form ((band1 – band 2)/ (band1 + band 2)) were used to detect the sensitive bands to SSC of soil samples. Optimal band combination that selected from the all of the waveband pairs that were band 683 and band 724 for difference form ($r = 0.538$) band 409 and band 723 for NDSI form ($r = 0.531$).

Correlation of the wavebands of measured salinities of 58 samples with all of the waveband pairs used in the difference form (Fig. 19-a) produced correlations (absolute value of $0.3 < r < 0.56$) for the following pairs: 400-700 nm and 702-799 nm (positive correlation), 405-768 nm and 713-798 nm (negative correlation), 680-780nm and 760-895nm (negative correlation). The bands pair have strongest correlation are band 724 and band 754 ($r = -0.56$), band 683 and band 724 ($r = 0.538$), band 409 and band 723 ($r = 0.53$).

Correlation of the wavebands of measured salinities of 58 samples with all of the waveband pairs used in the NDSI form (Fig. 19-b). The bands including wavelengths 409 and 723 nm ($r = 0.53$) were identified as the most promising bands that are sensitive to SSC.

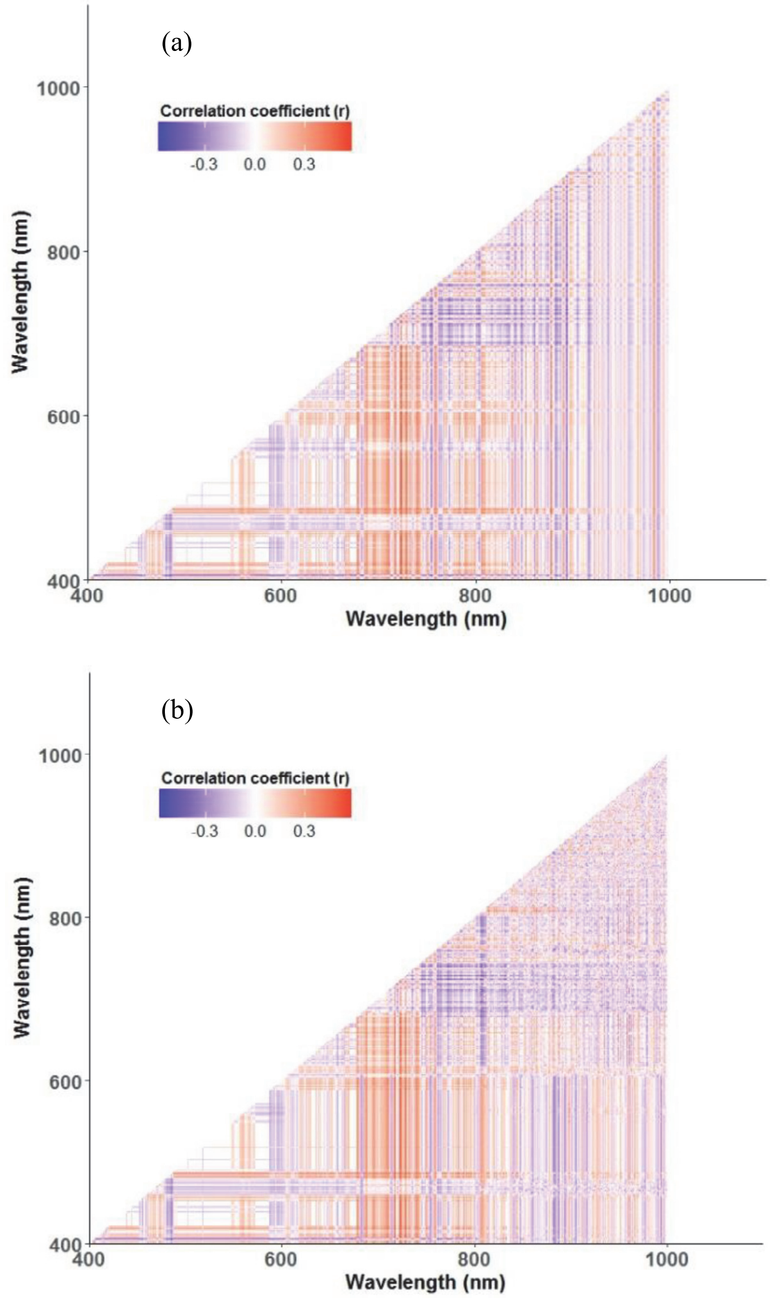

Fig. 19 (a) Heatmap of correlation coefficients (*r*) for measured salinities and all waveband pair's candidates from first derivate reflectance data in difference form (b) heatmap of correlation coefficients (*r*) for measured salinities and all waveband pairs from first derivate reflectance data candidates in NDSI form

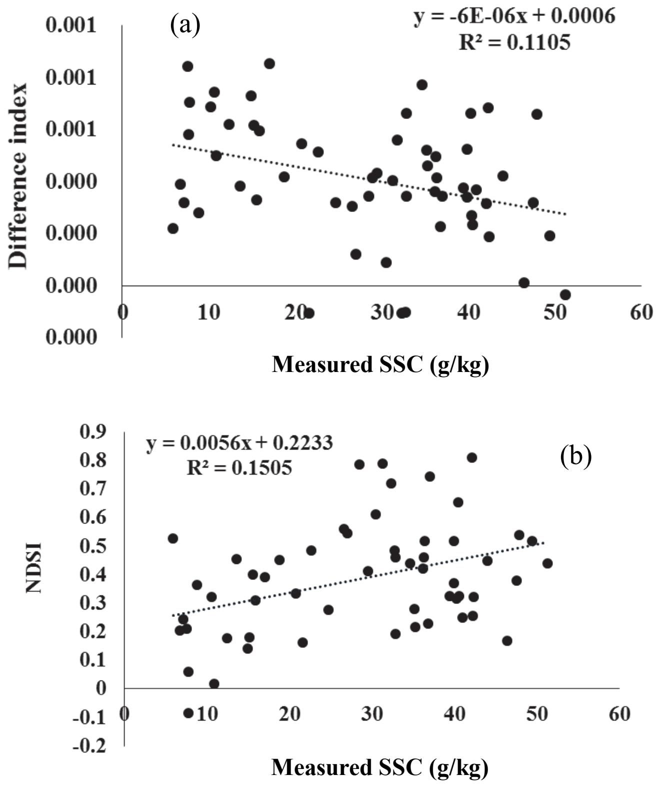

Fig. 20 (a) Scatter plot graph for measured salinities and difference index of first derivate reflectance data (b) scatter plot graph for measured salinities and NDSI of first derivate reflectance data.

27 samples were used for calibration. The correlation coefficients are 0.1105 and 0.1505 for difference index based calibration and NDSI based calibration (Fig. 20). The correlation between measured salinities and difference index of first derivate reflectance data and NDSI of first derivate reflectance data have poor modelling performances. The coefficients of both models were low, which indicated poor estimation ability of both index based modelling.

4.3.2.3 Continuum removed spectrum based modeling and model validation

The continuum removed spectrum have strengthen the absorption features of spectrum in terms of depth and width (Fig. 21-a). There were distinguished absorption region in the spectrum: 400-450 nm, 450-580 nm, 600-720nm, 750nm, 800-950nm. The correlation coefficient values of spectrum and SSC has high variation and change from negative to positive values (Fig. 21-b). However, compared to the original and first derivate reflectance, the correlation has been increased. The strongest negative coefficient was in the band of 569 with a value of -0.33 ($p > 0.05$) and strongest positive value in the band of 627 with a value of 0.494 ($p > 0.05$).

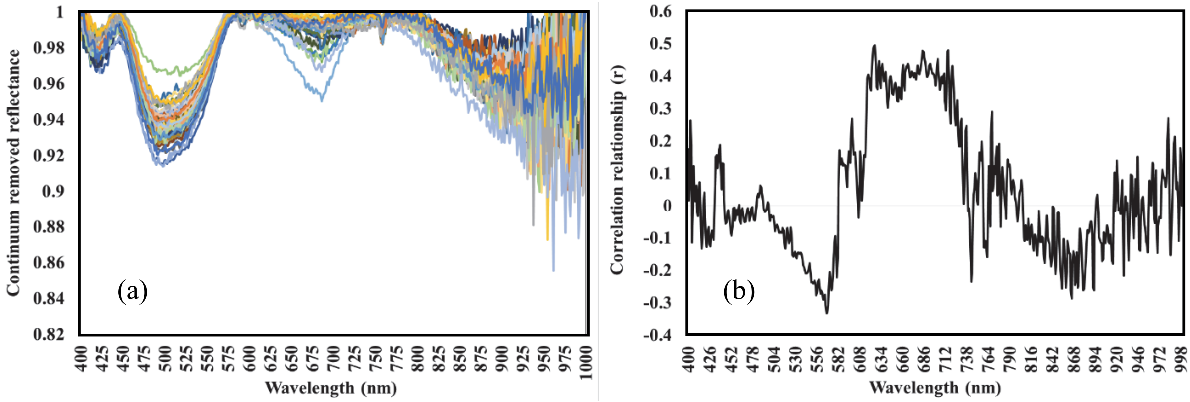

Fig. 21 (a) The spectrum of continuum removed reflectance for 58 soil samples (b) the correlation coefficient for continuum removed reflectance and SSC for 58 soil samples.

The sensitive band selection based on difference index (Fig. 22-a) and NDSI (Fig. 22-b) have obtained same results in terms of band pairs. Therefore, the correlation of the wavebands of measured salinities of 58 samples with all of the waveband pairs used in the NDSI (Fig. 22-b). 581-788 nm and 400-666 nm ($-0.3 < r < -0.53$), 600-700 nm and 700-900 nm ($0.3 < r < 0.587$). The bands pair of wavelengths 489 and 517 nm ($r = 0.587$) were identified as the most promising bands to use to develop a quantitative model for estimation of salt concentration from hyperspectral data.

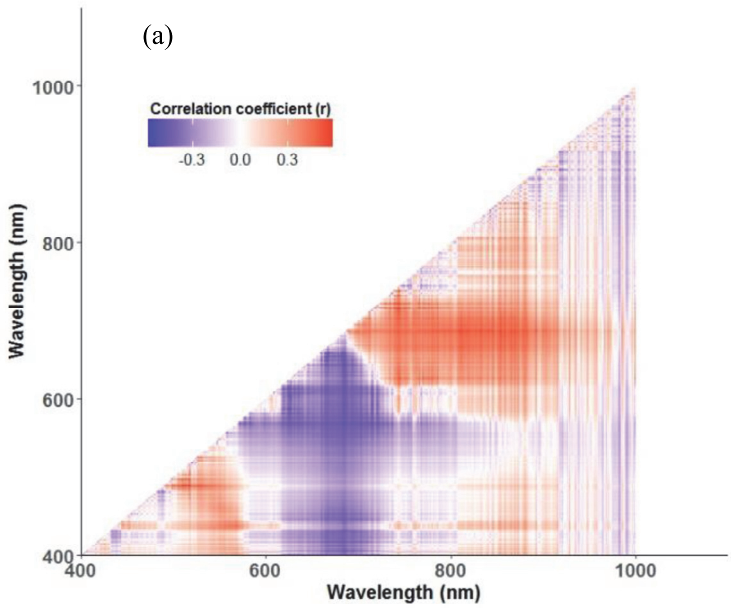

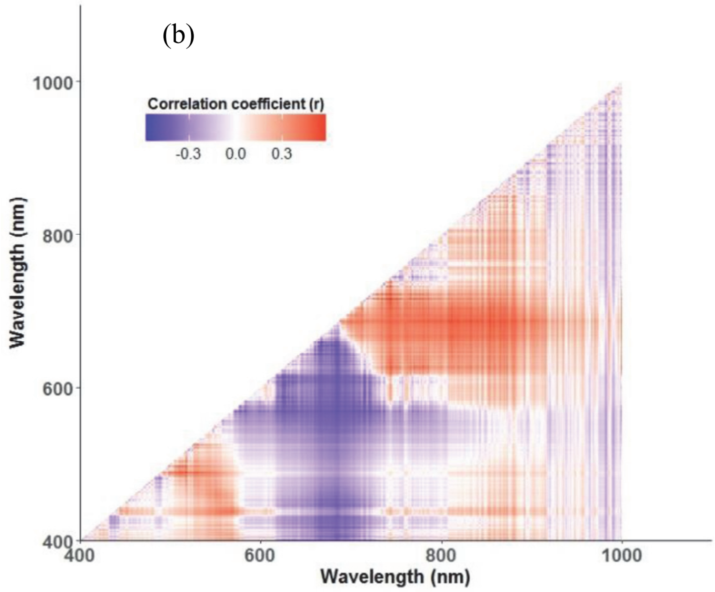

Fig. 22 (a) Heatmap of correlation coefficients (*r*) for measured salinities and all candidate waveband pairs in difference based on difference index, (b) heatmap of correlation coefficients (*r*) for measured salinities and all candidate waveband pairs in difference based on NDSI

We therefore defined the following normalized difference spectral index (NDSI):

$$NDSI2 = (B489 - B517) / (B489 + B517) \quad (7)$$

where B489 and B517 are CR-reflectance of spectral bands at 489 and 517 nm, respectively.

The model we established by univariate linear regression to 30 samples' estimate SSC from hyperspectral data (Fig. 23-a) was

$$SSC\ (g/kg) = -5223.3 \times NDSI2 + 40.261\ (R^2 = 0.2748) \quad (8)$$

Validation of the predicted values of SSC against measured values (Fig. 23-b) showed that Eq. 8 over-estimated SSC, which we attributed to the presence in our samples of some salt ions (e.g., Fe, Al) that were not measured during laboratory analysis.

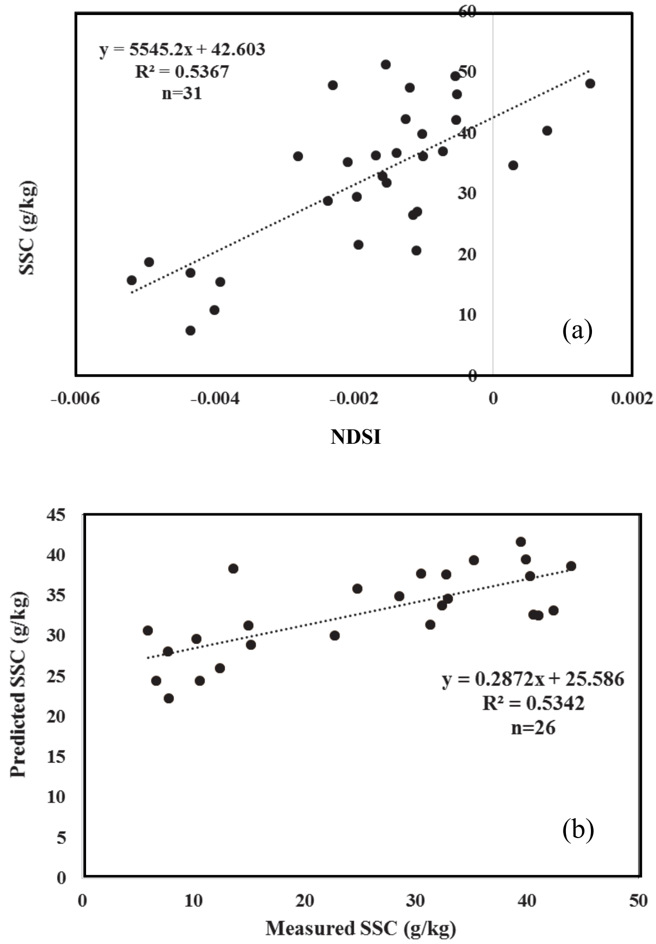

Fig. 23 (a) Measured soluble salt content (SSC) versus normalized difference spectral index (NDSI) and (b) scatter plot of measured SSC versus SSC estimated from Eq. 5.

The Fig. 24-a shows that the NDSI has no relationship with SMC. The residue of predicted SSC and measured SSC showed no relationship with SMC, which indicated the NDSI has removed the effect of soil salts on the spectrum and is directly responsible for soil salts (Fig. 24-b).

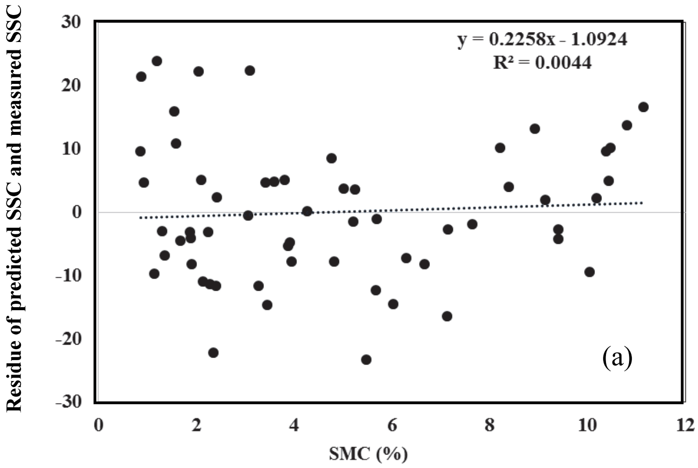

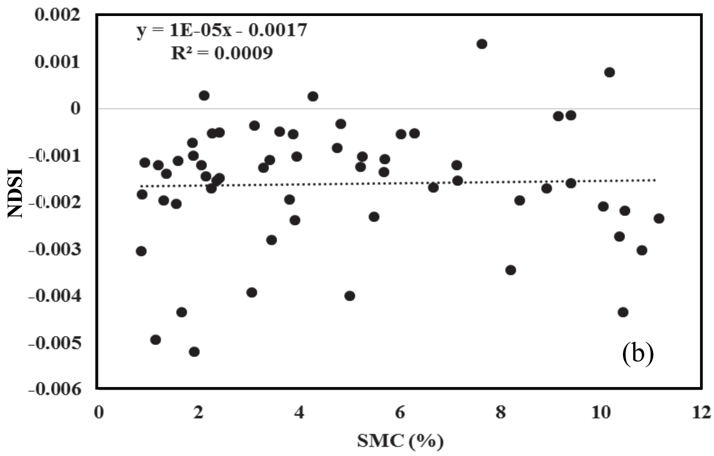

Fig. 24 (a) Soil moisture content (SMC) versus Residue of predicted SSC and measured SSC and (b) Soil moisture content (SMC) versus normalized difference spectral index (NDSI).

4.4 Results of principal component analysis

4.4.1 Extraction of PCA

13 component factors were selected as the best components (% of variance larger than 1%). The total variance explained are shown in Table 11

Table 11 Total variance explained

	Initial Eigenvalues			Extraction sums of squared loadings		
Factor	Total	% of Variance	Cumulative %	Total	% of Variance	Cumulative %
1	155.777	26.006	26.006	155.777	26.006	26.006
2	130.279	21.749	47.756	130.279	21.749	47.756
3	81.655	13.632	61.387	81.655	13.632	61.387
4	33.978	5.672	67.060	33.978	5.672	67.060
5	24.390	4.072	71.132	24.390	4.072	71.132
6	13.808	2.305	73.437	13.808	2.305	73.437
7	13.340	2.227	75.664	13.340	2.227	75.664
8	9.321	1.556	77.220	9.321	1.556	77.220
9	8.724	1.456	78.676	8.724	1.456	78.676
10	7.883	1.316	79.992	7.883	1.316	79.992
11	6.840	1.142	81.134	6.840	1.142	81.134
12	6.630	1.107	82.241	6.630	1.107	82.241
13	6.403	1.069	83.310	6.403	1.069	83.310

Extraction Method: Principal Component Analysis

The correlation (r) between soil properties and PCA factors shows that factor1 and factor 2 have stronger correlation with OMC (organic matter content) (factor 1, r = -0.480; factor 2, r = 0.321) and HCO_3^{-1} (factor 1, r = -0.367; factor 2, r = 0.387) and Ca (factor 1, r = 0.311); factor 3 has stronger correlation with SSC, EC and other soluble salts content; factor 7 has relatively strong correlation with SSC and other soluble salts content.

Table 12 The correlation between soil properties and PCA factors

	SSC	Na	K	Mg	Ca	Cl-	SO42-	HCO_3^{-1}	OMC	EC	pH	SMC
fac1	0.288	0.122	0.069	0.104	0.311	0.154	0.204	-0.367	-0.480	0.154	0.031	-0.400
fac2	-0.126	0.037	0.042	-0.024	-0.109	0.031	-0.188	0.387	0.321	0.007	0.253	0.163
fac3	0.374	0.290	0.397	0.190	0.378	0.267	0.162	-0.363	-0.086	0.321	0.115	-0.171
fac4	0.112	-0.007	0.033	-0.114	0.110	0.099	0.100	-0.150	0.070	-0.011	-0.039	-0.006
fac5	-0.117	-0.058	0.185	-0.186	-0.012	-0.070	-0.089	0.041	0.061	-0.071	0.051	0.078
fac6	-0.063	-0.046	-0.108	-0.132	-0.133	-0.128	0.022	0.113	0.127	-0.087	0.113	0.115
fac7	0.180	0.182	0.127	0.151	0.185	0.144	0.046	-0.049	0.105	0.190	0.115	0.241
fac8	-0.059	-0.075	-0.049	-0.116	-0.072	-0.056	0.001	0.094	0.011	-0.092	0.001	0.044
fac9	-0.020	0.170	0.151	0.200	0.036	0.081	-0.170	-0.002	-0.008	0.157	0.308	0.118
fac10	-0.083	-0.113	-0.319	-0.253	-0.158	-0.253	0.097	0.162	-0.049	-0.144	0.128	0.054
fac11	-0.097	0.075	0.078	-0.034	0.023	0.026	-0.187	0.121	-0.057	0.053	0.076	-0.006
fac12	0.098	0.210	0.197	0.214	0.147	0.167	-0.087	-0.118	0.098	0.214	-0.014	-0.107
fac13	-0.085	0.012	-0.058	0.084	-0.085	0.026	-0.121	0.012	0.079	0.012	0.187	0.015

4.4.2 Predictive regression models

Relationships between component factors and SSC have been quantified to predict soil salinity on the basis of stepwise regression models. The table 12 shows the result of stepwise regression analysis. Five models were extracted and the fifth model with constructed by 5 component factors (fac7, fac3, fac1, fac6, fac2) has the best performance. The 58 samples were divided into 2 groups including calibration. The calibration data contains 30 samples.

Table 13 ANOVA

Model		Square of root	Degree of freedom	Mean square	F	Significant level
1	Regression	1142.360	1	1142.360	9.068	.005[b]
	Residue	3653.187	29	125.972		
	Total	4795.547	30			
2	Regression	1754.852	2	877.426	8.080	.002[c]
	Residue	3040.695	28	108.596		
	Total	4795.547	30			
3	Regression	2220.553	3	740.184	7.761	.001[d]
	Residue	2574.995	27	95.370		
	Total	4795.547	30			
4	Regression	2582.873	4	645.718	7.588	.000[e]
	Residue	2212.675	26	85.103		
	Total	4795.547	30			
5	Regression	2922.231	5	584.446	7.800	.000[f]
	Residue	1873.316	25	74.933		
	Total	4795.547	30			

a. depended variable：SSC

b. predictors: (constant), fac7

c. predictors: (constant), fac7, fac3

d. predictors: (constant), fac7, fac3, fac1

e. predictors: (constant), fac7, fac3, fac1, fac6

f. predictors: (constant), fac7, fac3, fac1, fac6, fac2

The coefficients of models are shown in the following tables:

Table 14 The coefficients of models [a]

Model		Unstandardized Coefficients		Standardized Coefficients	t	Sig.
		B	Std.Error	Beta		
1	(constant)	32.268	2.033		15.876	.000
	fac7	6.453	2.143	.488	3.011	.005
2	(constant)	31.235	1.937		16.129	.000
	fac7	5.364	2.042	.406	2.627	.014
	fac3	5.679	2.391	.367	2.375	.025
3	(constant)	30.868	1.822		16.938	.000
	fac7	4.020	2.008	.304	2.002	.055
	fac3	7.966	2.468	.514	3.227	.003
	fac1	4.374	1.980	.350	2.210	.036
4	(constant)	30.823	1.722		17.903	.000
	fac7	4.540	1.913	.343	2.373	.025
	fac3	9.082	2.394	.587	3.794	.001
	fac1	4.899	1.887	.392	2.596	.015
	fac6	3.937	1.908	.289	2.063	.049
5	(constant)	31.053	1.619		19.179	.000
	fac7	5.247	1.826	.397	2.874	.008
	fac3	8.882	2.248	.574	3.951	.001
	fac1	5.260	1.779	.421	2.957	.007
	fac6	4.797	1.835	.353	2.613	.015
	fac2	-3.900	1.832	-.279	-2.128	.043

a. depended variable：SSC

Based on the coefficients, five models were extracted. The models are:

y1 = 32.268+6.453* fac7;

y2 = 31.235+5.364* fac7+5.679* fac3;

y3 = 30.868+4.020* fac7+7.966* fac3+4.374* fac1;

y4 = 30.823+4.540* fac7+9.082* fac3+4.899* fac1+3.937* fac6;

y5 = 31.053 + 5.247* fac7 + 8.882* fac3 + 5.260* fac1 + 4.797* fac6 - 3.900* fac2.

4.4.3 Validation of models

After removing 2 outliers, the remaining 25 samples were used to validate the models. The results indicate that the prediction models could not predict the SSC of soils well.

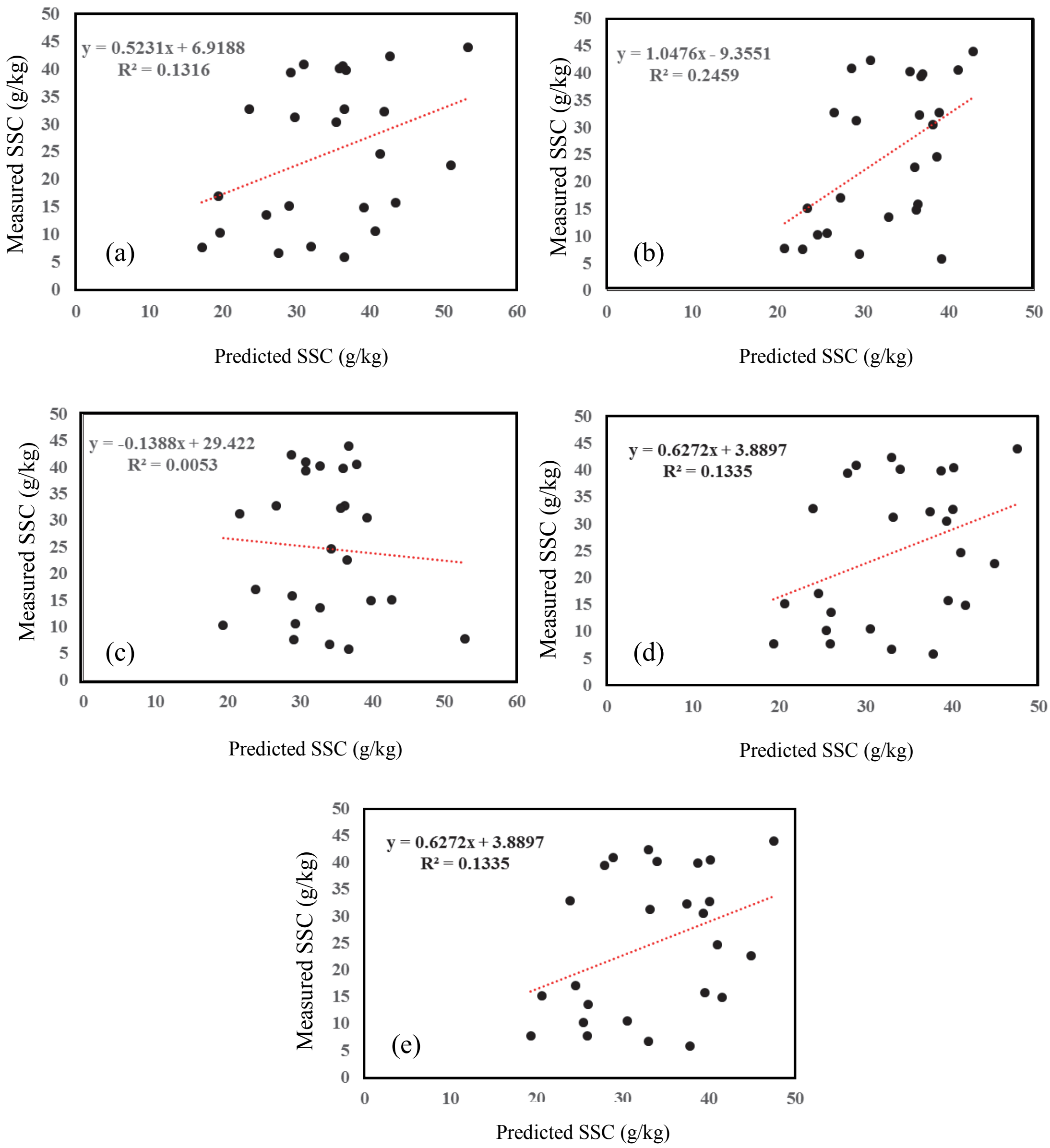

Fig. 25 (a) the calibration of model1, (b) the calibration of model 2, (c) the calibration of model 3, (d) the calibration of model 4, (e) the calibration of model 5.

4.4 Comparison between field-spectra-based retrieval model and lab-spectra-based retrieval model

Band 489 and 517 were selected as optimal bands for retrieving salinity from field spectra, while band 1358 and band 2382 were selected as optimal bands for retrieving salinity from lab spectra. A cross combination of 2 bands from field and lab spectra was band 489 and band 1358, and the other combination was band 517 and band 2382.

We therefore defined the following NDSI3 and NDSI4:

$$NDSI3 = (B_f 489 - B_l 1358) / (B_f 489 + B_l 1358),$$

$$NDSI4 = (B_l 2382 - B_f 517) / (B_l 2382 + B_f 517), \quad (6)$$

where B_f 489, B_f 517, B_l 1358 and B_l 2382 are CR-reflectance of spectral bands at 489 and 517 from field, 1358 and 2382 nm from laboratory, respectively.

Fig. 25-b showed that the NDSI4 formed by band 517 and 2382 has stronger correlation relationship with soluble salt content (SSC) than NDSI3 formed by band 489 and 1358 (Fig. 25-a). Therefore, we used the NDSI4 to establish the univariate linear regression model to estimate SSC from hyperspectral data (Fig. 26-b):

$$SSC\ (g/kg) = 1351.6 \times NDSI4 - 7.0429\ (R^2 = 0.2695). \quad (7)$$

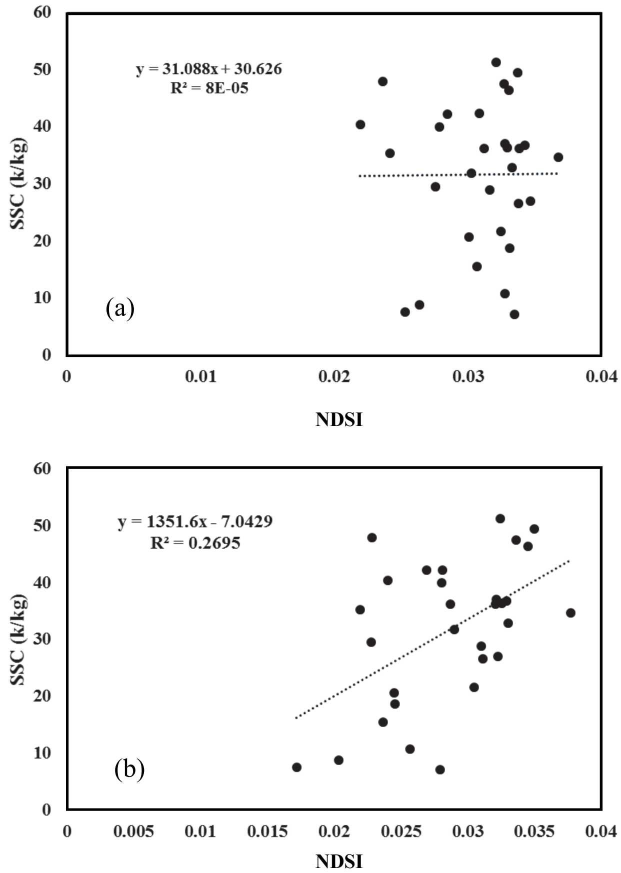

Fig. 26 (a) Measured soluble salt content (SSC) versus normalized difference spectral index (NDSI) formed by band 489 and 1358 (b) Measured soluble salt content (SSC) versus normalized difference spectral index (NDSI) formed by band 517 and 2382.

Validation of the predicted values of SSC against measured values (Fig. 27) showed that the cross-combination of band 2382 and 517 performed poorer prediction than band 489 and 517, which indicated that combining field and lab spectra unable to improve that accuracy of retrieving soil salinity.

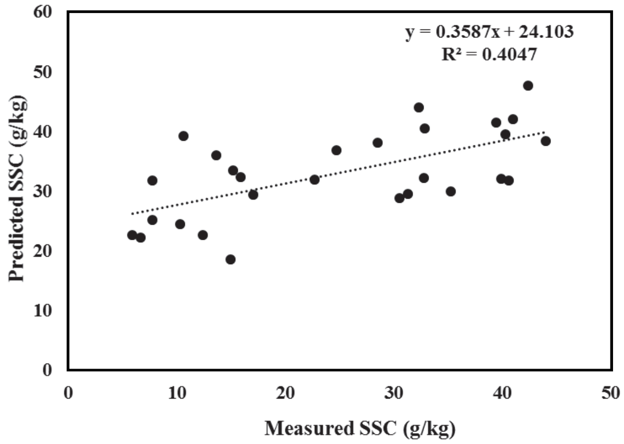

Fig. 27 Measured soluble salt content (SSC) versus predicted soluble salt content (SSC).

4.5 Conclusions

We used 58 samples of surface soil in the Huqu region of Minqin oasis. A normalized difference spectral index of salinity that integrates any two randomly selected hyperspectral bands was used to obtain all possible waveband pairs that might be associated with the soluble salt content.

Correlation analysis of the indexes obtained for all of the possible waveband pairs from 400-1000 nm wavelength with the corresponding measured soil salinities for all of the 58 samples showed that, compared with original spectra, first derivate spectra, the continuum-removed spectra showed stronger correlation with soluble salt content and band 489 and 517 were selected as optimal bands for retrieving salinity from continuum-removed field spectra. We applied linear regression modelling to these bands to construct a spectral index. Validation of the index by correlation analysis of the index-derived salt content with measured salt content of 31 soil samples showed a relative strong correlation (R^2 = 0.4819). The PCA analysis and cross-field-and-laboratory-spectra analysis failed to perform satisfied prediction modelling.

Chapter 5

General conclusions

Chapter 5 General conclusions

Salt-affected soils were widely distributed throughout the Huqu area. Laboratory chemical analyses of the samples showed that the dominant salts were chlorine and sulphate compounds Most of the cropland had relatively low soil salinity, but several samples had high $EC_{1:5}$, which indicates a high potential for secondary salinization. The saline wasteland had some of the highest salinity values, and was concentrated mainly at the margin of the oasis (probably dried wetland, lake, abandoned croplands), where there was no irrigation for recent decades and close to the natural salinized condition. Secondary salinized land was mainly located in areas of sparse grassland inside the oasis. The CV values of soil $EC_{1:5}$ for cropland and shrubland were greater than 1.0, which indicates that soil $EC_{1:5}$ and its distribution were strongly influenced by human activities. Land-use practices also strongly influenced the distribution of salt-affected soils. The abandoned cropland had low salinity, but the long-abandoned cropland (which became sparse grassland) tended to have high salinity, sometimes reaching values as high as those in saline wasteland. In addition, transforming cropland to shrubland could result in further land degradation in Huqu area due to the water scarcity and poor irrigation water quality.

Among those factors that affecting spatial distribution and degree of soil salinity, the distance to the nearest irrigation canal was the most important factor for determining the salinity of cropland. The access to fresh river water and good drainage, combined with a deep groundwater table, prevented salt accumulation in the topsoil. However, the use of highly saline water and improper drainage and soil management will increase the risk of secondary salinization in irrigated soils. Therefore, proper irrigation methods, an improved drainage system, and effective soil management will be necessary to prevent non-salinized cropland from undergoing secondary salinization and to remediate existing salinized cropland.

We measured spectral reflectance for soil samples both in field and laboratory. The equipment are different for field and laboratory spectrum. Field spectrum has a wavelength of 325-1350 nm while the laboratory spectrum has a wavelength of 350-2350 nm. All the spectrum were pre-processed by continuum-removed analysis. We developed a normalized difference spectral index that integrates any two randomly selected hyperspectral bands to obtain all possible waveband pairs that might be associated with the salts contributing to salinization. Correlation analysis was conducted for the indexes obtained for all of the possible waveband pairs with the corresponding measured soil salinities for all the samples.

The laboratory spectrum analysis results showed that two bands centred at 2382 and 1358 nm were closely associated with soil salts content. Validation of the linear regression model by correlation analysis of the index-derived salt content with measured salt content showed a strong correlation (R^2 = 0.8272).

The field spectrum analysis results showed that two bands centred at 489 and 517 were selected as optimal bands for retrieving salinity from continuum-removed field spectra. Validation of the index by correlation analysis of the index-derived salt content with measured salt content of 31 soil samples showed a relative strong correlation (R^2 = 0.4819).

Through the comparison of the modelling of two different set of data (field and laboratory), firstly, the continuum-removed analysis was approved appropriate for correlation analysis and modelling process; secondly, based on limited wavelength NIR spectra data obtained from field, the retrieving of soil salinity can obtain relative good results; as last, using the full wavelength spectra data obtained from laboratory measurement would improve the ability to retrieve the soil salinity and perform better soil salts estimation.

Further research is needed on the application of this method to remotely sensed (aircraft or satellite) digital hyperspectral data so that its potential use for large-scale predictive mapping of the extent and severity of soil salinity can be investigated.

References

Aslam M. and Prathapa S. A. 2006. Strategies to mitigate secondary salinization in the Indus Basin of Pakistan: A selective review. International Water Management Institute research report, Colombo, Sri Lanka (97). International Water ManagementInstitute, Colombo

Douaoui A. E. K., Nicolasb H. and Walter C. 2006. Detecting Salinity Hazards within a Semiarid Context by Means of Combining Soil and Remote-Sensing Data. Geoderma, 134(1-2): p.217-230.

Adhikari P., Shukla M. K. and Mexal J.G. 2011. Spatial variability of electrical conductivity of desert soil irrigated with treated wastewater: Implications for irrigation management. Applied and Environmental Soil Science, 504249 (2011): pp. 1-11.

Asib A., 2011. Some of the major environmental problems relating to land use changes in the coastal areas of Bangladesh: A Review Journal of Geography and Regional Planning, 4(1): p.1-8.

Singh A., Sudhindra N. P., Wolfgang-albert F. and Peter K. 2012. Waterlogging and farmland salinisation: causes and remedial measures in an irrigated semi-arid region of India. Irrigation of Drainage, 61 (3): p.357-365.

A. Allbed and L. Kumar. 2013. Soil Salinity Mapping and Monitoring in Arid and Semi-Arid Regions Using Remote Sensing Technology: A Review. Advances in Remote Sensing, 2 (4): p.373-385.

Beven K. J. and Kirkby M. J. 1979. A physically based, variable contributing area model of basin hydrology. Hydrological Sciences Bulletin, 24(1): p. 43-69.

Brower C., Goffeau A. and Heilbloem M. 1985. Irrigation Water Management: Irrigation Scheduling, Training manual No. 1- Introduction to Irrigation, FAO, Rome, Italy.

Ben-Dor E. and Banin A. 1995. Near-Infrared Analysis as a Rapid Method to Simultaneously Evaluate Several Soil Properties. Soil Science Society of America Journal, 59: p.364-372.

Boroson, T. A., & Green, R. F. 1992, ApJS, 80, 109 (BG92)

Bao S. D. 2000. Soil Agricultural Chemistry Analysis. Beijing: China Agriculture Press, p.178–198 (in Chinese).

Ben-Dor E., Patkin K., Banin A. and Karnieli A. 2002. Mapping of several soil properties using DAIS-7915 hyperspectral scanner data - a case study over clayey soils in Israel. International

Journal of Remote Sensing, 23(6): p.1043-1062.

Barrett-Lennard E. G. 2003. The interaction between waterlogging and salinity in higher plants: causes, consequences and implications. Plant and Soil, 253(1): p.35-54.

Berry L. 2003. Land degradation in China: its extent and impact. Global Mechanism of the United Nations Convention to Combat Desertification (UNCCD). Bonn, Germany.

Ben-Dor E., Chabrillat S., Demattê J. A. M., Taylor G.R., Hill J., Whiting M.L. and Sommer S. 2009. Using Imaging Spectroscopy to study soil properties. Remote Sensing of Environment, 113(Supplement 1): S38-S55.

Bondes M. and Li D. 2013. Climate Change and Sustainable Development in Western China's Minqin Oasis: Joining Forces with Society. In: Vajpeyi D. Climate Change. Sustainable Development and Human Security. New York: Lexington, p.139-168.

Clark R. N. and Roush T. L. 1984. Reflectance spectroscopy: Quantitative analysis techniques for remote sensing applications. Journal of Geophysical Research: Solid Earth, 89(B7): p.6329-6340.

Crowley J. K. 1991. Visible and near-infrared (0.4–2.5 um) reflectance spectra of Playa evaporate minerals. Journal of Geophysical Research: Solid Earth, 96(B10): p.16231-16240.

Csillag F., Pásztor L. and Biehl, L. L. 1993. Spectral band selection for the characterization of salinity status of soils, Remote Sensing of Environment, 43(3): p.231–242.

Chang Z. F., Liu H.J., Zhao M., Han F. G. and Zhong S. N. 2007. A primary study on the process of formation and succession of desert vegetation in Minqin. Journal of Arid Land Resources and Environment, 21(7): p.116-124. (In Chinese).

Chen L., Feng Q., Li C.S., Song Y.X., Liu W., Si J.H. and Zhang B.G. 2016. Spatial Variations of Soil Microbial Activities in Saline Groundwater-Irrigated Soil Ecosystem. Environmental Management, 57(5): p.1054-1061.

Drees L.R. and Wilding L.P. 1983.Microradiography as a submicroscopic tool Geoderma, 30 (1983):p. 65-76.

Deng J. L. 1989. Introduction to Grey system theory. Journal of Grey System, 1(1): p. 1-24.

Dwivedi R. S. 2001. Soil resources mapping: A remote sensing perspective. Remote Sensing Reviews, 20(2): p.89-122.

Dehaan R and Taylor G. R. 2003. Image-derived spectral endmembers as indicators of salinization. International Journal of Remote Sensing, 24(4): p.775-794.

Douaoui A E K, Nicolas H. and Walter C. 2006. Detecting salinity hazards within a semiarid context by means of combining soil and remote-sensing data. Geoderma, 134(1): p.217-230.

Sun D. F., S., Dawson R. and Baoguo L. 2006. Agricultural causes of desertification risk in Minqin, China. Journal of Environmental Management, 79(4): p.348-356.

Ding J. L., Wu M. C. and Tiyip T. 2011. Study on soil salinization information in arid region using remote sensing technique. Agricultural Sciences in China, 10(3): p.404-411.

Danner M., Locherer M., Hank T. and Richter K. 2015. Spectral Sampling with the ASD FieldSpec4-Theory, Measurement, Problems, Interpretation. GFZ Data Services. Brandenburg, Germany.

Ernandez-Bucs N., Siebe C., Cram S. and Palacio L. 2006. Mapping soil salinity using a combined spectral response index for bare soil and vegetation: A case study in the former lake Texcoco, Mexico. Journal of Arid Environments, 65(4): p.644-667

Elnaggar A.A. and Noller J.S., Application of remote-sensing data and decision-tree analysis to mapping salt-affected soils over large areas. Remote Sensing, 2009. 2(1): p.151-165.

Farifteh J., Farshad A. and George R. J. 2006. Assessing salt-affected soils using remote sensing, solute modelling, and geophysics. Geoderma, 130(3): p.191-206.

Fernandez-Buces, N., Siebe C., Cram S. and Palacio J., 2006. Mapping soil salinity using a combined spectralresponse index for bare soil and vegetation: A case study in the former lake Texcoco, Mexico. Journal of Arid Environments, 65: p.644–667.

Farifteh J., Van der Meer F., Atzberger C. and Carranza E. J. M. 2007. Quantitative analysis of salt-affected soil reflectance spectra: A comparison of two adaptive methods (PLSR and ANN). Remote Sensing of Environment, 110(1): 59-78.

Farifteh J., Van der Meer F., Van der Meijdeb M. and Atzbergerc C. 2008. Spectral characteristics of salt-affected soils: A laboratory experiment. Geoderma, 145(3): p.196-206.

Fan X., Liu Y., Tao J. and Weng Y. 2015. Soil Salinity Retrieval from advanced multi-spectral sensor with partial least square regression. Remote Sensing, 7(1): p.488-511.

Goetz A. E. H. 1989. Spectral remote sensing in geology. In: Ghassem A. Theory an Application of Optical Remote Sensing, NY: John Wiley and Sons, p.491-526.

Gessler P.E., Oliver A., C., Chamran F., Lynnedee A. and Karen W. H. 2000. Modeling soil–landscape and ecosystem properties using terrain attributes. Soil Science Society of America Journal, 64(6): p.2046-2056.

Greiner R. 1998. Catchment management for dryland salinity control: Model analysis for the Liverpool Plains in New South Wales, Agricultural Systems, 56: p.225-251.

Gomez C., Viscarra R. A. and McBratney A. B. 2008. Soil organic carbon prediction by hyperspectral remote sensing and field vis-NIR spectroscopy: An Australian case study. Geoderma, 146(3): p.403-411.

Goetz A. F. H. 2009. Three decades of hyperspectral remote sensing of the Earth: A personal view. Remote Sensing of Environment, 113(Supplement 1): S5-S16.

Gao Y.F., Wang J. and He Z. D. 2013. Grey correlation analysis on influencing factors of postgraduates' innovative capacity. Journal of Theoretical and Applied Information Technology, 49(1): p.419-425

Hunt G. R. and Salisbury J. W. 1970. Visible and near infrared spectra of minerals and rocks: I. Silicates. Modern Geology 1: p.283-300.

Hunt G. R. and Salisbury J. W. 1971. Visible and near infrared spectra of minerals and rocks: II. Carbonates. Modern Geology 2: p.23-30.

Hunt, G. R., Salisbury J. W. and Lenhoff C. J. 1971a. Visible and near infrared spectra of minerals and rocks: III. Oxides and hydroxides. Modern Geology 2: p.195-205.

Hunt G. R., Salisbury J. W. and Lenhoff C. J. 1971b. Visible and near infrared spectra of minerals and rocks: IV. Sulfides and sulfates. Modern Geology 3: p.1-14.

Hunt G. R., Salisbury J. W. and Lenhoff C. J. 1972. Visible and near infrared spectra of minerals and rocks: V. Halides, phosphates, arsenates, vanadates and borates. Modern Geology 3: p.121-132.

Hunt G. R. and Salisbury J. W. 1976.Visible and near infrared spectra of minerals and rocks: XI. Sedimentary rocks. Modern Geology 5: p.211-217.

Hunt G. R. 1977. Spectral signatures of particulate minerals in the visible and near infrared. Geophysics, 42(3): p.501.

Howari F. M., Goodell P. C. and Miyamoto. S. 2002. Spectral Properties of Salt Crusts Formed on Saline Soils. Journal of Environmental Quality, 31: p.1453-1461.

Huang Z., Brian J., Turner S. J., Dury. R. W. and Foley W. J. 2004. Estimating foliage nitrogen concentration from HYMAP data using continuum removal analysis. Remote Sensing of Environment. 93(1): p.18-29.

Haubrock S. N., Sabine C., Matthias K., Patrick H. and Hermann K. 2008. Surface soil moisture quantification and validation based on hyperspectral data and field measurements. Journal of applied remote sensing, 2(1): p.1-26

Huang J., 2011. Employing the grey system theory to explore the effect of RFID on the quality of life among older adult users. Journal of Statistics and Management Systems, 14(1): p.217-228.

Hillel D. 2000. Salinity Management for Sustainable Irrigation. The World Bank, Washington D. C. I. Shainberg, G. J. Levy, Salination Processes, Encyclopedia of Soils in the Environment, Elsevier, p.429-435.

Kahle A. B. 1982. Spectral remote sensing of rocks in arid lands. ERIM, First Thematic Conference: Remote Sensing of Arid and Semi-Arid Lands, Jan. (19-25), Cairo, Egypt, p.279-295.

Kang S., Su X., Tong L., Shi P., Yang X., Abe Y., Du T., Shen Q. and Zhang J. 2004. The impacts of human activities on the water–land environment of the Shiyang River basin, an arid region in northwest China. Hydrological Sciences Journal, 49(3): p.427.

Karim Z., Hussain S.G. and Ahmed M., 1990. Salinity problems and crop intensification in the coastal regions of Bangladesh, Dhaka, BARC Soils publication (33).

Kayacan E., Ulutas B. and Kaynak O. 2010. Grey system theory-based models in time series prediction. Expert Systems with Applications, 37(2): p.1784-1789.

Kargas G, Chatzigiakoumis I, Kollias A, Spiliotis D and Kerkides P. 2018. An Investigation of the Relationship between the Electrical Conductivity of the Soil Saturated Paste Extract ECe with the Respective Values of the Mass Soil/Water Ratios 1:1 and 1:5 (EC1:1 and EC1:5). Proceedings, 2(11):661.

Lin S. J., Lu I. J. and Lewis C. 2007. Grey relation performance correlations among economics, energy use and carbon dioxide emission in Taiwan. Energy Policy, 35(3): p.1948-1955.

Lu P., Wang L., Zheng N. Li L. and Zhang W. 2013. Prediction of soil properties using laboratory VIS–NIR spectroscopy and Hyperion imagery. Journal of Geochemical

Exploration, 132(Supplement C): p.26-33.

Li J, Pu L., Han M. Zhu M. Zhang R. and Xiang Y. 2014. Soil salinization research in China: Advances and prospects. Journal of Geographical Sciences, 24(5): p.943-960.

Local chronicles office of Minqin Count., Annals of Shi Yang River. 2014: Wuwei Guangxin Kemao Printing Co., Ltd.: p.295-296.

Luo S. M. and Stephen R. 2016. Gliessman Agroecology in China: Science, Practice, and Sustainable Manageme, Boca Raton: CRC Press, p.321-321.

Lv Q., Jiang L., Ma B., Zhao B. and Huo Z. 2018. A study on the effect of the salt content on the solidification of sulfate saline soil solidified with an alkali-activated geopolymer, Construction and Building Materials, (76): p.68-74,

Maas E.V., Poss J. A. and Hoffman G.J. 1986. Salinity sensitivity of sorghum at three growth stages. Irrigation of Science, (7):p.1-11.

Moore I. D., Grayson R. B. and Ladson A. R. 1991. Digital terrain modelling: a review of hydrological, geomorphological, and biological applications. Hydrological Processes, 5(1): p.3-30.

Mougenot B., Pouget M. and Epema G. F. 1993. Remote sensing of salt affected soils. Remote Sensing Reviews, 7(3-4): p.241-259.

Munns R. 2002. Comparative physiology of salt and water stress. Plant, Cell and Environment, 25(2): p.239-250.

Metternicht G. I. and Zinck J. A. 2003. Remote sensing of soil salinity: potentials and constraints. Remote Sensing of Environment, 85(1): p.1-20.

Ma J. Z., Wang X. S. and Edmunds W. M. 2005. The characteristics of ground-water resources and their changes under the impacts of human activity in the arid Northwest China—a case study of the Shiyang River Basin. Journal of Arid Environments, 61(2): p.277-295.

Ma Y., Fan S., Zhou L., Dong Z. Zhang K. and Feng J. 2007. The temporal change of driving factors during the course of land desertification in arid region of North China: the case of Minqin County. Environmental Geology, 51(6): p.999-1008.

Mohamed S.I., Mohamed A.R., Mohammad S., Nahid N., Biswajit P. and Alak P. 2012. Using geospatial techniques to assess the salinity impact on agricultural landuse: a study on

Shyamnagar Upazila, Satkhira. Journal of Agriculture and Environment for International Development, 106 (2): p.157-169

Mashimbye Z. E. 2013. Remote sensing of salt-affected soils. Doctoral dissertation. Western Cape: Stellenbosch University.

Marthews T.R., Dadson S. J., Lehner B., Abele S. and Gedney N. 2015. High-resolution global topographic index values for use in large-scale hydrological modelling. Hydrology and Earth System Sciences, 2015. 19(1): p.91-104.

Nurmemet I., Ghulam A., Tiyip T., Elkadiri R., Ding J. L. and Maimaitiyiming M., Abdulla A., Mamat S., Fei Z., Abdugheni A. and Qian S. 2015. Monitoring soil salinization in Keriya River Basin, north western China using passive reflective and active microwave remote sensing data. Remote Sensing. (7): p.8803–8829.

Pitman MG and Läuchli A. 2002. Global impact of salinity and agricultural ecosystems. In: Läuchli A, Lüttge U, eds. Salinity: Environment – Plants – Molecules. Dordrecht, the Netherlands: Kluwer, p.3–20.

Pichu R. 2006. World salinization with emphasis on Australia, Journal of Experimental Botany, 57 (5): p.1017–1023.

Paul B. and Rashid H. 2016. Climatic Hazards in Coastal Bangladesh: Non-Structural and Structural Solutions, 1st ed.; Butterworth-Heinemann: Oxford, UK.

Qian T., Tsunekwa A., Masunaga T. and Wang. T. 2017. Analysis of the Spatial Variation of Soil Salinity and Its Causal Factors in China's Minqin Oasis. Mathematical Problems in Engineering, (2017): 1-9

Rengasamy P. 2006. World salinization with emphasis on Australia. Journal of experimental botany, 57(5): p.1017-1023.

Szabolcs I. 1989. Salt-affected soils. Boca Raton, Fl: CRC Press.

Sumner M.E., Rengasamy P. and Naidu R. 1998. Sodic soils: a reappraisal. In: Sumner ME and Naidu R (eds) Sodic Soils, New York: Oxford University Press, pp. 3–17

Solomon H., Li Z., Yamamoto S. Yang S. L., Peng L. and Waleed H. A. E. H. 2005.Classification of salinization processes in Luohui Irrigation Scheme, China - Part of water management research to prevent salinization in semiarid land. Journal of Arid Land Studies, 15(2): p.89-105, Shainberg I. and Levy G. J. 2005. Salination processes, Encyclopedia of Soils in the Environment.p.429-435.

Schmid T., Gumuzzio. J., Koch M., Mather O. and Solana J. 2007. Characterizing and monitoring semi-arid wetlands using multi-angle hyperspectral and multispectral data. In proceedings of Envisat Symposium 2007, ESA SP-636, Montreux, Switzerland, p.1-6.

Sheng J., Ma L., Jiang P., Li B., Huang F. and Wu H. 2010. Digital soil mapping to enable classification of the salt-affected soils in desert agro-ecological zones. Agricultural Water Management, 97(12): p.1944-1951.

Shepherd K. D. and Walsh M. G. 2002. Development of reflectance spectral libraries for characterization of soil properties. Soil Science Society of America Journal (66): p.988-998.

Sallehuddin R., Shamsuddin S. M. H. and Hashim S. Z. M. 2008. Application of grey relational analysis for multivariate time series. In Proc. Int. Conf. on Intelligent Systems Design and Applications (ISDA'08), (2), Kaohsiung, Taiwan, p. 432-437.

Song S., Zhao X., Xie J. and Guan Y. 2011. Grey Correlation Analysis and Regression Estimation of Mining Subsidence in Yu-Shen-Fu Mining Area. Procedia Environmental Sciences, (10): p.1747-1752.

Singh A. 2010. Decision support for on-farm water management and long-term agricultural sustainability in a semi-arid region of India Journal of Hydrology, 391 (1–2), p.63-76.

Singh A. 2011. Estimating long-term regional groundwater recharge for the evaluation of potential solution alternatives to waterlogging and salinization. J. Hydrol., 406 (3–4): p.245-255

Scudiero E., Skaggs T. H. and Corwin D. L. 2016. Comparative regional scale soil salinity assessment with near ground apparent electrical conductivity and remote sensing canopy reflectance. Ecological Indicators, (70): p.276–284.

Thomas G. W. 1996. Soil pH and Soil Acidity. In: Sparks R S L, Swift D. L. Methods of Soil Analysis. Part 3-Chemical Methods, Soil Science Society of America, p.475-490.

Wilding L. P. and Drees L. R. 1983. Spatial variability and pedology. Developments in Soil Science, (11): p.83-116.

Wang Z. 1993. Chinese saline-alkaline soil. Beijing: Science Press. p.335 (in Chinese).

Walker L. E. 1999. Psychology and domestic violence around the world. American

Psychologist. 54(1): p.21–29.

Wild A. 2003. Soils, Land and Food-Managing the Land during the 21st Century. Cambridge: Cambridge University Press, p.84-85.

Wang Y., Li Y. and Xiao D. 2008. Catchment scale spatial variability of soil salt content in agricultural oasis, Northwest China. Environmental Geology, 56(2): p.439-446.

Weng Y., Gong P. and Zhu Z. 2010. A Spectral Index for Estimating Soil Salinity in the Yellow River Delta Region of China Using EO-1 Hyperion Data. Pedosphere, 20(3): p.378-388.

Wang Q., Li P. and Chen X., 2012. Modelling salinity effects on soil reflectance under various moisture conditions and its inverse application: A laboratory experiment, Geoderma, (170): p.103-111.

Wei H., Ya L., Cundong X., Lanping Z., Xiaoke H., Feng D. and Fang C. 2016. The Process of Cultivated Land and Water Resource Distribution Changing in Recent Decades in Upstream and Downstream in Shiyang Inland River Basin in Arid Area of Northwest China. Journal of Geoscience and Environment Protection, 4(7): p.166-171.

Wang, Y., Caiyun D., Yan L., Ziru N. and Yan L. 2018. Identifying change in spatial accumulation of soil salinity in an inland river watershed, China. Science of The Total Environment, (621): p.177-185.

Xiao D., Li X., Song D. and Yang G. 2007. Temporal and spatial dynamical simulation of groundwater characteristics in Minqin Oasis. Science in China Series D: Earth Sciences, 50(2): p.261-273.

Yan N., Marschner P., Cao W., Zuo C. and Qin W. 2015. Influence of salinity and water content on soil microorganisms. International Soil and Water Conservation Research (3):p.316–323.

Zhang F., Tashpolat T., Jianli D., Hsiangte K.,Verner C. J,, Mamat S., Nigara T. and Dongwei G. 2003. Studies on the reflectance spectral features of saline soil along the middle reaches of Tarim River: a case study in Xinjiang Autonomous Region, China. Environmental Earth Sciences, 69(8): p.2743-2761.

Zornoza R., Guerrero C., Mataix-Solera J., Scow K.M., Arcenegui V. and Mataix-Beneyto J. 2008. Near infrared spectroscopy for determination of various physical, chemical and biochemical properties in Mediterranean soils. Soil Biology and Biochemistry, 40(7): p.1923-1930.

Zhang L., Yang S. and Zhang M. 2014. Study on land use change in arid and semiarid region based on GIS--RS. Information Technology Journal, 13(8): p.1567-1571.

Zhang J. 2014. Salt-Affected Soil Resources in China. In: Jianfeng Zhang. Coastal Saline Soil Rehabilitation and Utilization Based on Forestry Approaches in China. Berlin: Springer Science & Business Media, p.9-13.

SUMMARY

Dryland salinity is the most common type of land degradation encountered in natural resource management in many semi and arid land of the world and has received much attention from farmers, politicians and researchers. As one of the primary inhibitors of crop yield and ecological functions, soil salinity might ultimately lead to environmental disaster and food crises in arid regions. Soil salinization is a serious ecological and environmental problem because it adversely affects sustainable development worldwide, especially in arid and semi-arid regions. Soil salinization in China occurs mainly in arid and semi-arid areas in the north-western region, where low precipitation is coupled with intensive evaporation and ineffective irrigation drainage systems have resulted in secondary salinization. The semi-arid and arid land in China are mainly in Northwest region and the area of salt-affected soils counts about37.4% of total area of salt-affected soil.

Minqin oasis, the study area, is located in the lower reaches of an inland river of northwest China, suffers a great shortage of fresh water for agriculture because of the low rainfall and massive demand for water created by increased agricultural activity and rapid population growth. Soil salinization and water resource deterioration negatively affect the local irrigated agriculture semi-arid areas by limiting the area of arable land and reducing crop yields. Groundwater has been over-exploited to fill the gap between surface freshwater supply and demand. Groundwater extraction provides short-term relief from the scarcity of water for agricultural and domestic use, but excessive extraction lowers the water table and increases salt concentrations in groundwater. Long-term agricultural use of saline water has led to a rapid increase of secondary salinization, which also led to land abandonment and threaten the crop production and agriculture system. Damage to the environment has been extensive, and represents a serious threat to the sustainability of social and economic development in the Minqin oasis.

Monitoring and accurate estimates of the areal extent of salinized land and prediction of salt-affected areas are essential for policy makers, planners and farmers to allow effective management of irrigated land, control of salinization and reversal of current trends of soil and water degradation, and achieve sustainability of agriculture.

However, the conventional methods of monitoring salinity by using ground-based geophysical techniques are time-consuming and costly. Multispectral data has been used widely for capture the salt-affected area. However, due to limited spectral resolution, it is difficult to clarify the non-saline and slightly-saline soils. Hyperspectral remote sensing techniques has been used to detect soil salinity and monitor soil salinization efficiently and widely with high spectral resolution and range. It can capture the spectral characteristics (peak and absorption) of salts for characterizing soil salinity and distinguishing different levels of soil salinity.

Therefore, the aim of this thesis is to develop predictive models for quantifying salts content in soils on the basis of the using of soil hyperspectral reflectance and field survey in Minqin oasis. The specific objectives are: (a) to qualitatively mapping the salinity and analyzing its casual factors; (b) to quantitatively estimate soil salinity by modeling from lab-measured spectral reflectance data; (c) to quantitatively estimate soil salinity by modeling from field-measured spectral reflectance data.

The study comprises 3 studies as follows:

The introductory section of this study was presented. It sets out an overview of the background for the study, focusing on the adverse effect of soil salinization problems, review of previous researches related with monitoring salinization technology (conventional and advanced modern technology), literary review and the methods that used to salinization detection and prediction. Subsequently, it presents the study objectives and organization of the thesis.

Firstly, Secondly, spatial variation of soil salinity and its causal factors were analyzed. obtained 94 surface soil samples were collected to a depth of 10 cm from unused land (9 samples from shrubland, 5 samples from abandoned land, 46 samples from sparse grassland, 13 samples from saline wasteland) and cropland (used to grow wheat, sunflower, alfalfa, goji

berry, and fennel). The saline-alkaline land were mainly concentrated in the margin of oasis without human intervention (affected by micro topographic and hydrological factors). Secondary salinized land mainly located in the long-term abandoned land inside the oasis. Land-use practices had a crucial influence on the distribution and accelerating soil salinization. Through the grey relation analysis among soil salinity and other possible casual factors include underground water table, distance to irrigation cannels, topography index and vegetation coverage. The distance to irrigation cannels has been identified as the key casual factor for salinization, which indicated that access to the fresh irrigation water resource is the key factor for improving salinization in Minqin.

Secondly, the salt content were derived in salinized soil from hyperspectral reflectance data which has a full wavelength (350nm-2500nm) and measured in lab-condition. Lab-condition ignored the soil water moisture and atmospheric factors that could lead to noise in reflectance. During April 2015 we collected surface soil samples (0–10 cm depth) at 64 field sites of Minqin oasis undergoing NaCl and $CaSO_4$ salinization. We used a normalized difference spectral index (NDSI) of salinity that integrates any two randomly selected hyperspectral bands to obtain all possible waveband pairs that might be associated with the salts contributing to salinization. Correlation analysis of the indexes obtained for all of the possible waveband pairs with the wavebands corresponding to the measured soil salinities showed that two bands centered at 2382 and 1358 nm were closely associated with sodium and chloride concentrations. We applied linear regression modelling to these bands to construct a normalized difference spectral index. Validation of the index by correlation analysis of the index-derived salt content with measured salt content of 31 soil samples showed a strong correlation (R^2 = 0.8272). Thus, the model (SSC [g/kg] = 5312.3 $\times NDSI_{2382:1358}$ + 34.2) we derived successfully estimated the salt content of surface soils in the study area.

Thirdly, differed set of hyperspectral reflectance data which has a full wavelength (350nm-1000nm) was used to derive the salt content in salinized soil from and measured in field-condition that is different with lab-condition. Based on the correlation analysis with $EC_{1:5}$, the sensitive bands pair at 489 and 517 nm were selected successfully. The model obtained was (SSC [g/kg] = -5223.3 $\times NDSI_{489:517}$ + 40.3 (R^2=0.275). The pre-process includes continuum-removed analysis and first derivation were separately applied to spectrum, and the results indicated that continuum-removed analysis give a better performance on removing noise of spectrum. In addition, based on the comparing between 2 different dataset, using the full wavelength spectra data based on the pre-process of continuum-removed analysis would improve the ability to retrieve the soil salinity and perform better soil salts estimation.

To sum up, in this study, based on the strong relationship between soluble salt content and spectral reflectance, the sensitive wavelength were successfully selected. NDSI was developed from the selected wavelength and applied to predict the soluble salt content.

学位論文概要

世界の乾燥地では、塩類集積による農業生産力の低下が大きな問題となっている。中国では塩類集積の影響を受けている土地は、その 69%が北西部に集中している。民勤（ミンチン）オアシスは、中国北西部の甘粛省に位置し、祁連山脈を源とする石羊河の下流域にある。民勤オアシスでは大規模な灌漑農業が行われているが、土壌の塩類化が進行しており、放棄された耕地が年々増えている。そのため塩類集積地の広がりとその程度を正確に把握することが塩害に対する適切な対策を取る上で喫緊の課題となっている。

塩類集積地の状況を把握するには、現地調査で採取した土壌の塩分を測定する方法が一般的である。しかしこのような現地調査にもとづく方法は、その結果を得るために多くの時間と費用を要する。そこで時間的・経済的効率性に優れる衛星リモートセンシングによる塩類集積地の把握に関する研究が進められてきた。しかし、塩類の分光反射特性は全域において比較的平坦な特性を持つので、従来の多波長帯での観測データを利用する方法では、塩分濃度を定量的に推定することはむずかしい。そこで、電磁波を計測する際の分光波長帯（バンド）を数 nm 程度の精度で刻み、数百のバンドで観測するハイパースペクトルリモートセンシングの利用が検討されてきている。ハイパースペクトルリモートセンシングでは、土壌の反射率から微細な分光反射特性を抽出することで、土壌状態の詳細な解析が可能となる。塩類の種類等によって、その分光反射特性も異なるため、植生指数のように一般的に用いられる指数はこれまで開発されていない。

そこで本研究では、民勤オアシス北部の湖区を対象として、ハイパースペクトルデータを用いて、土壌の塩分濃度を推定することを目的とした。具体的には、①民勤オアシスの塩類土壌の分布状況の把握およびその塩類化要因の解明、②実験室で測定された土壌の分光反射率を用いた土壌塩分濃度の推定、③野外で測定された土壌の分光反射率を用いた土壌塩分濃度の推定という三つの課題に取り組んだ。本論文の主たる成果は以下の通りである。

第一に、塩類土壌の分布状態と塩類化要因を分析した。塩類集積状況を把握するため，94 個の表層土サンプルを採取し、$EC_{1:5}$、pH、土壌水分含量等を分析した。そして、地下水位、灌漑水路までの距離、地形指標（CTI）、植物被覆率などの要因と土壌の $EC_{1:5}$ との関係をグレイ相関分析により解析した。その結果、塩類土壌は多様な分布状況を示し、$EC_{1:5}$ と最も相関の高い要因は灌漑水路までの距離であった。

第二に、実験室で測定された土壌の分光反射率を用いて土壌塩分濃度を推定するため、64 個の表層土壌サンプルを採取し、実験室で $EC_{1:5}$、Na^+、K^+、Mg^{2+}、Ca^{2+}、$Cl-$、SO_4^{2-}、HCO_3^-、CO_3^{2-}、有機物含量等を分析した。合わせて各サンプルの分光反射率を分光放射計（波長範囲：350nm～2500nm）で計測した。計測された分光反射率を用いて作成された正規化分光指数と土壌塩分濃度との相関関係を IDL により解析した。正規化分光指数（Normalized Difference SpectralIndex: NDSI）とは、正規化差分により定義される指数で、二つのバンド｀の反射率の差を±1 の範囲に正規化した値である。その結果、土壌塩分

濃度と強い相関を持つ 1358nm と 2382nm を中心とする二つのバンドが選択された。この 2 バンドを用いた NDSI と土壌塩分濃度（SSC）との線形回帰分析を行って、土壌試料の土壌塩分濃度を推定する予測式（$SSC[g/kg]=5312.3\times NDSI_{2382:1358}+34.2$（$R^2=0.827$））を得た。

第三に、携帯型分光放射計（波長範囲：325nm～1075nm）を用いて野外で 59 点の土壌サンプルの分光反射率を計測し、持ち帰った土壌サンプルについて 2 と同様の土壌化学性を分析した。計測された分光反射率に対して、包絡線の除去と 1 次微分などの前処理を行って、測定ノイズの影響を軽減する効果を比べた結果、包絡線の除去が最適だと判断された。また土壌塩分濃度と最も相関の高い 489nm と 517nm を中心とする二つのバンドの組み合わせを用いて土壌塩分濃度を推定する予測式（$SSC[g/kg]=-5223.3\times NDSI_{489:517}+40.3$（$R^2=0.275$））を得た。

以上を要するに、本研究の成果は、土壌塩分濃度と強い相関を持つ分光波長帯を特定し、正規化分光指数を用いて土壌塩分濃度を推定する手法を導いたことである。

LIST OF PUBLICATIONS

Tana QIAN, Atsushi TSUNEKAWA, Tsugiyuki MASUNAGA, and Tao WANG. 2017. Analysis of the Spatial Variation of Soil Salinity and Its Causal Factors in China's Minqin oasis. Mathematical Problems in Engineering, Volume 2017, 1-9 (Published online, https://doi.org/10.1155/2017/9745264, this article covers **Chapter 2**).

Tana QIAN, Asushi TSUNEKAWA, Fei PENG, Tsugiyuki MASUNAGA, Tao WANG and LI Rui. 2018. Derivation of salt content in salinized soil from hyperspectral reflectance data: A case study at Minqin oasis, northwet China. Journal of Arid Land (Accepted, this article covers **Chapter 3**).